

1 **Contribution of HONO to the atmospheric oxidation capacity in an industrial zone**
2 **in the Yangtze River Delta region of China**

3 Jun Zheng^{1*}, Xiaowen Shi¹, Yan Ma^{1,2}, Xinrong Ren^{3,4,5}, Halim Jabbour¹, Yiwei Diao^{1,6}, Weiwei Wang⁶, Yifeng
4 Ge¹, Yuchan Zhang¹, and Wenhui Zhu¹

5 ¹Collaborative Innovation Center of Atmospheric Environment and Equipment Technology, Nanjing University
6 of Information Science & Technology, Nanjing 210044, China

7 ²NUIST Reading Academy, Nanjing University of Information Science & Technology, Nanjing 210044, China

8 ³Air Resources Laboratory, National Oceanic and Atmospheric Administration, College Park, Maryland, USA

9 ⁴Department of Atmospheric and Oceanic Science, University of Maryland, College Park, Maryland, USA

10 ⁵Cooperative Institute for Satellite Earth System Studies, University of Maryland, College Park, Maryland, USA

11 ⁶Key Laboratory for Aerosol-Cloud-Precipitation of China Meteorological Administration, Department of
12 Atmospheric Physics, Nanjing University of Information Science and Technology, Nanjing 210044, China

13

14 *Correspondence to: Dr. Jun Zheng (zheng.jun@nuist.edu.cn)*

15 *Address: School of Environmental Science and Engineering, Nanjing University of Information*

16 *Science & Technology, Nanjing 210044, China*

17 *Tel.: +86-18251919852*

18 *Fax: +86-25-58731090*

19

20 **Key points:**

- 21 • High levels of HONO, with an average of 1.32 ± 0.92 ppbv, were observed near one of the largest industrial
22 zones in the YRD region of China.
- 23 • HONO photolysis and alkene ozonolyses contributed the most of OH production and hence the atmospheric
24 oxidation capacity.
- 25 • High loading of PM_{2.5} provided additional reaction surfaces for HONO formation.
- 26 • Heterogeneous formation mechanisms were the most important daytime HONO sources and were further
27 enhanced by sunlight.

28 **Abstract**

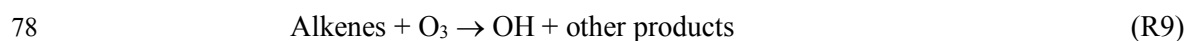
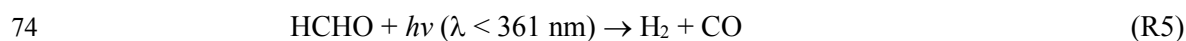
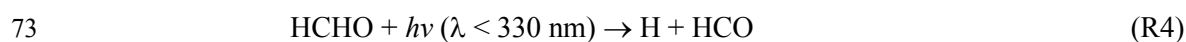
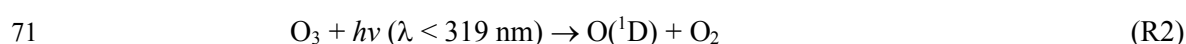
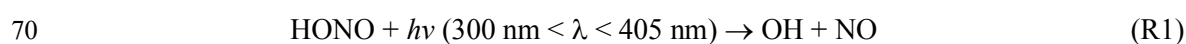
29 A suite of instruments were deployed to simultaneously measure nitrous acid (HONO), nitrogen oxides (NO_x
30 = NO + NO₂), carbon monoxide (CO), ozone (O₃), volatile organic compounds (VOCs, including formaldehyde
31 (HCHO)) and meteorological parameters near a typical industrial zone in Nanjing of the Yangtze River Delta region,
32 China, from 1 to 31 December 2015. High levels of HONO were detected using a wet chemistry-based method.
33 HONO ranged from 0.03-7.04 ppbv with an average of 1.32 ± 0.92 ppbv. Elevated daytime HONO was frequently
34 observed with a minimum of several hundreds of pptv on average, which cannot be explained by the homogeneous
35 OH + NO reaction ($P_{\text{OH}+\text{NO}}$) and primary emission (P_{emission}), especially during periods with high loadings of
36 particulate matters (PM_{2.5}). The HONO chemistry and its impact on atmospheric oxidation capacity in the study
37 area were further investigated using a MCM-box model. The results show that during the campaign period the
38 average hydroxyl radical (OH) production rate was dominated by the photolysis of HONO (7.13×10^6 molecules
39 $\text{cm}^{-3} \text{s}^{-1}$), followed by ozonolysis of alkenes (3.94×10^6 molecules $\text{cm}^{-3} \text{s}^{-1}$), photolysis of O₃ (2.46×10^6 molecules
40 $\text{cm}^{-3} \text{s}^{-1}$) and photolysis of HCHO (1.60×10^6 molecules $\text{cm}^{-3} \text{s}^{-1}$), especially within the plumes originated from the
41 industrial zone. Model simulations indicated that heterogeneous chemistry played an important role in HONO

42 formation. The average nighttime NO_2 to HONO conversion rate was determined to be $\sim 0.8\% \text{ hr}^{-1}$. Good correlation
43 between nocturnal HONO/ NO_2 and the product of particle surface area density (S/V) and relative humidity (RH),
44 S/V·RH, supports the heterogeneous $\text{NO}_2/\text{H}_2\text{O}$ reaction mechanism. The other HONO source, designated as
45 P_{unknown} , was about twice as much as $P_{\text{OH}+\text{NO}}$ on average and displayed a diurnal profile with an evidently photo-
46 enhanced feature, i.e., photosensitized reactions of NO_2 may be an important daytime HONO source. Nevertheless,
47 our results suggest that daytime HONO formation was mostly due to the light-induced conversion of NO_2 on aerosol
48 surfaces but heterogeneous NO_2 reactions on ground surface dominated nocturnal HONO production. Our study
49 indicated that elevated $\text{PM}_{2.5}$ level during the haze events can promote NO_2 to HONO conversion by providing
50 more heterogeneous reaction sites and hence increase the atmospheric oxidation capacity, which may further
51 promote the formation of secondary air pollutants.

52 **1 Introduction**

53 Nitrous acid (HONO) plays an important role in tropospheric photochemistry because its fast photolysis
54 contributes to the formation of hydroxyl (OH) radical, which is an essential atmospheric oxidant that initiates the
55 oxidation of volatile organic compounds (VOC) to form organic peroxy radicals (RO_2) and hydroperoxyl radical
56 (HO_2). In the presence of nitrogen oxides ($\text{NO}_x = \text{NO} + \text{NO}_2$), these free radicals are the fundamental driving force
57 of photochemical reaction cycles that lead to the formation of ground-level ozone (O_3) and secondary organic
58 aerosols (SOA) (Finlayson-Pitts and Pitts, 1999; Xue et al., 2016). Besides HONO photolysis (R1), the major
59 known OH radical initiation sources include photolysis of O_3 (R2 and R3) and formaldehyde (HCHO) (R4 to R8),
60 and ozonolysis of alkenes (R9) (Finlayson-Pitts and Pitts, 1999). Nevertheless, many field studies have
61 demonstrated that HONO may strongly affect atmospheric oxidation capacity in various environments (Bernard et
62 al., 2016; Elshorbany et al., 2009; Elshorbany et al., 2010; Zhou et al., 2002). In early studies, HONO was believed
63 to be only important as NO_x reservoir during nighttime, when HONO can accumulate in the atmosphere and give

64 a boost of photochemistry in the following early morning (Platt et al., 1980). However, recent field studies have
65 demonstrated that high concentrations of HONO are often present in the relatively polluted urban areas during the
66 day. Because of high levels of HONO, the photolysis of HONO becomes an important OH source not only in the
67 early morning but also throughout the day and can contribute up to 30-90% of OH radical during daytime (Acker
68 et al., 2006; Hendrick et al., 2014; Kleffmann et al., 2005; Neftel et al., 1996; Spataro et al., 2013; Su et al., 2008;
69 Zhou et al., 2002).



79 Despite the significance of HONO in daytime photochemistry, the sources and formation mechanisms of
80 HONO, especially during daytime, are still uncertain. Traditionally, the reaction between NO and OH was thought
81 to be the most important homogeneous source for HONO (Perner and Platt, 1979):



83 However, reaction R10 alone cannot sustain the high HONO level observed during daytime in many studies, in
84 which the observed HONO levels were often an order of magnitude greater than the modeled HONO with only
85 homogeneous HONO source (R10) included in the model (Ren et al., 2010; Tang et al., 2015). Nevertheless, higher
86 than expected OH observed in several studies (Hofzumahaus et al., 2009) may explain partially observed higher

87 than model predicted HONO levels. It has been suggested that HONO may be emitted directly by incomplete
88 combustion processes, such as vehicle exhaust (Kirchstetter et al., 1996; Kurtenbach et al., 2001; Liang et al., 2017;
89 Nakashima and Kajii, 2017; Trinh et al., 2017; Xu et al., 2015) and biomass burning (Müller et al., 2016; Neuman
90 et al., 2016; Nie et al., 2015; Rondon and Sanhueza, 1989). However, such strong but sporadic point sources could
91 not account for the widely observed daytime HONO in the polluted areas (Elshorbany et al., 2012; Wang et al.,
92 2017). Recently, many other HONO formation pathways have been proposed. Su et al. (2011) pointed out that
93 HONO can be released from soil nitrite, which was formed through biological nitrification and denitrification
94 processes. Recent studies demonstrated that the pH and organic content of soil could influence the HONO emission
95 rate (Scharko et al., 2017; Sörgel et al., 2015). In addition, vertical profiles of HONO measurements indicated that
96 HONO was very likely originated from the ground surface (Kleffmann et al., 2003; VandenBoer et al., 2013; Wong
97 et al., 2011; Wong et al., 2013). However, the presence of in-situ HONO sources in the air masses aloft cannot be
98 ruled out (Wong et al., 2013; Zhang et al., 2009).

99 Several heterogeneous processes have been drawn substantial attention and are proposed as the major HONO
100 sources, including: (1) heterogeneous conversion of NO_2 on wet surface (Finlayson-Pitts et al., 2003), which could
101 be an important nocturnal HONO source; (2) NO_2 heterogeneous reaction with fresh soot particles (Ammann et al.,
102 1998; Gerecke et al., 1998; Han et al., 2017a; Monge et al., 2010) and semi-volatile organic compound emitted
103 from diesel exhausts (George et al., 2005; Gutzwiller et al., 2002), which could be an important process because it
104 is 1 to 2 orders of magnitude faster than the typically proposed heterogeneous reaction of $2\text{NO}_2 + \text{H}_2\text{O}$; (3)
105 photosensitized reaction of NO_2 on surfaces of mineral dust (Ndour et al., 2008), humic acid (Han et al., 2017b;
106 Wall and Harris, 2016), and ground surface (i.e., certain reactions such as $\text{NO}_2 + \text{humic acids}$ on ground surfaces)
107 (Wong et al., 2012), which has been considered as an important daytime HONO source (Lee et al., 2016); (4)
108 photolysis of adsorbed nitric acid (HNO_3) and nitrate (NO_3^-) (Ye et al., 2016; Ye et al., 2017; Zhou et al., 2002;
109 Zhou et al., 2003; Zhou et al., 2011; Ziemba et al., 2010); (5) VOC-mediated conversion of HNO_3 into HONO

110 (Gall et al., 2016).

111 Since the first atmospheric HONO measurement by Nash (1974) and the first use of long path differential UV
112 absorption technique (LP-DOAS) to measure atmospheric HONO (Perner and Platt, 1979), various measurement
113 techniques for HONO have been developed, such as spectroscopic techniques, wet chemistry-based techniques,
114 and chemical ionization mass spectrometry (CIMS). Besides DOAS technique, other spectroscopic techniques such
115 as the cavity ring-down spectroscopy (Rairoux et al., 2002), the incoherent broadband cavity-enhanced absorption
116 spectroscopy (IBBCEAS) (Gherman et al., 2008), and the cavity-enhanced absorption spectrometer (CEAS)
117 (Scharko et al., 2017) were applied in the HONO measurements. Wet chemistry techniques have the advantages of
118 higher sensitivity and lower detection limit, including long path absorption photometer (LOPAP) (Heland et al.,
119 2001; Kleffmann et al., 2003; Kleffmann et al., 2005; Kleffmann et al., 2006; Kleffmann and Wiesen, 2008; Vecera
120 and Dasgupta, 1991), AIM-IC analysis system and wet-rotating-denuder (WRD) method (Makkonen et al., 2012).
121 Very recently, CIMS techniques have been developed for fast on-line HONO measurements (Bernard et al., 2016;
122 Pinto et al., 2014; Ren et al., 2010).

123 Yangtze River Delta (YRD) region is the largest industrial zone in China and is experiencing ever increasing
124 air pollution events, characterized with high ozone (O_3) and fine particulate matters ($PM_{2.5}$) concentrations (Ding
125 et al., 2013). Despite of the great efforts in reducing sulfur dioxide (SO_2) and NO_x emissions from industrial
126 activities, high level of NO_x along with ammonia/amines have been observed near an industrial park (Zheng et al.,
127 2015b). In addition, high levels of HCHO have been frequently observed near industrial zones in China (Ma et al.,
128 2016; Wang et al., 2015b), providing an extra radical source. HONO concentrations calculated using a
129 photostationary state (PSS) approach that included homogeneous sources were found much less HONO than the
130 measured values during daytime (Kleffmann et al., 2005; Michoud et al., 2014). Lee et al. (2016) conducted a
131 detailed analysis of HONO budget and proposed that the missing daytime HONO source was related to NO_2 and
132 sunlight. A four-season measurement campaign was carried out in an urban site of Beijing and the results showed

133 monthly averaged HONO concentrations between 1.05 and 2.27 ppbv with pronounced seasonal profile (Wang et
134 al., 2017). In a recent study, Nie et al. (2015) revealed the influence of biomass burning on HONO formation at a
135 suburban site of Nanjing and demonstrated that the contribution of heterogeneous conversion of NO₂ to HONO
136 formation. However, so far, no comprehensive study on the oxidizing capability, i.e., the major contributors of OH
137 radicals, has ever been conducted in the industrial zone of YRD region.

138 In this work, we have performed HONO measurements using a custom-built wet chemistry-based method at
139 an industrial site in December 2015 in Nanjing, China. In addition, HCHO, O₃, photolysis frequencies, other trace
140 gases and meteorological parameters were also measured. The contributions of HONO along with other OH sources
141 to OH budget were investigated using a box model based on Master Chemical Mechanism (MCM). The
142 mechanisms of possible daytime HONO formation and the consequent impacts on air pollutants formation were
143 explored.

144

145 **2 Experimental and Model Description**

146 **2.1 HONO Measurement**

147 The field measurements were carried out from 1 to 31 December 2015 on the campus of Nanjing University
148 of Information Science and Technology (NUIST) in Nanjing, China. More details about the observation site have
149 been provided in our previous work (Ma et al., 2016; Zheng et al., 2015b). Briefly, the site is located to the west of
150 clusters of steel mills and petrochemical refinery facilities and is about 15 km to the north of the downtown Nanjing.
151 All instruments were placed inside an air-conditioned trailer. In this study, a custom-built wet chemistry-based
152 HONO instrument was utilized for HONO measurements, which was originally developed by Ren et al. (2010).
153 Figure 1 is the schematics of the HONO instrument, consisting of two sample collection glass coils connected

154 successively, a 10-port injection valve (Valco Instruments Co. Inc.), a 1-m long liquid waveguide capillary cell
155 (LWCC, World Precision Instruments), and a mini spectrometer (Ocean optics, USB4000). Two coil samplers in
156 serial were used to measure total signals in the first sampler and the background in the second sampler. The
157 difference between the two samplers is the net HONO signal. The background signal is usually only a few percent
158 of the total signal.

159 To minimize the sampling artifacts, the sampling coils were set up about 3.5 m above the ground (1.5 m above
160 the trailer rooftop) and no inlet was used. Ambient air was pulled through the coils by a vacuum pump at 1 L min⁻¹,
161 which was controlled by a mass flow controller (MKS, model M100B). In the first coil, HONO along with some
162 interfering species in the air sample were separated from the gas phase and transformed into nitrite solution by a
163 1.0 mmol L⁻¹ phosphate buffer scrubbing solution. Potential interfering species (e.g., NO₂) would also interact with
164 scrubbing solution in the second coil in a similar way as in the first coil. The nitrite solutions from the two coils
165 were then respectively mixed with sulfanilamide/N-(1-naphthyl) ethylene-diamine (SA/NED) reagents in Teflon
166 derivatization tubing and nitrite was converted via the two reactions (SR1 and SR2, see the SI for details) (Huang
167 et al., 2002). The aqueous sample was injected into the LWCC and the produced azo dye was quantified by its
168 absorption at 560 nm with a mini USB spectrometer. The difference between the absorbance signals of the two
169 coils was treated as the actual HONO signal. The HONO mixing ratio in ambient air was calculated using Eq. (1):

$$170 \quad [\text{HONO}]_{\text{pptv}} = \frac{C_1 F_l R T}{F_g P} \times 10^{12} \quad (1)$$

171 where, C_1 is nitrite concentration (mol L⁻¹) in the scrubbing solution, F_l is the liquid flow rate (mL min⁻¹) of the
172 scrubbing solution, F_g is the sampling air flow rate (L min⁻¹), R is the ideal gas constant (8.314 m³ Pa K⁻¹mol⁻¹),
173 and T and P are the ambient temperature (294 K) and atmospheric pressure (101325 Pa), respectively, under which
174 the mass flow controller (MFC) that was used to control the sample flow rate was calibrated (Ren et al., 2010). The
175 instrument calibration was carried out once every four days by injecting standard sodium nitrite (NaNO₂) solution
176 into the instrument right after the sampling coil. According to the calibration curve, HONO mixing ratio in ambient

177 air can be quantified. The detection limit of the HONO instrument was about 3 pptv with a time resolution of 2
178 min. The measurement accuracy was about $\pm 15\%$ at a 95% confidence level (Ren et al., 2010).

179 **2.2 Other measurements**

180 As the observation site was part of a national standard meteorology observatory facility, meteorology
181 parameters, including wind direction, wind speed, ambient temperature, pressure and RH were continuously
182 measured. Trace gases, CO (Thermo Scientific, Model 48i), O₃ (Thermo Scientific, Model 49i), SO₂ (Thermo
183 Scientific, Model 43i) and NO_x (Thermo Scientific, Model 17i) were also measured at the observation site. The
184 Thermo Scientific 17i is designed as an ammonia (NH₃) analyzer. It basically consists of a typical NO_x analyzer
185 and an external high temperature (700°C) NH₃ converter, which is disabled and bypassed in this work. Therefore,
186 it was used as a typical NO_x analyzer. It is well known that a NO-NO_x analyzer with a molybdenum-based converter
187 can convert portion of NO_z (=NO_y-NO_x) to NO, which can then be detected as NO₂ causing an interference in NO₂
188 measurement (Villena et al., 2012). However, an aircraft study conducted in the eastern US in the winter 2015
189 found that within 6 hours of transport time, NO_x account for more than 90% of NO_y in an urban outflow (Salmon
190 et al., 2018). A sensitivity analysis showed that by decreasing the NO₂ level of 10% (an upper limit assuming all
191 NO_z were converted into NO with an efficiency of 100%), the modeled HONO decreased only by 5.3%, indicating
192 that the possible small interference in NO₂ measurement did not impact significantly on the modeled HONO results.
193 The details about the operation and calibrations of these instruments were described in previous work (Zheng et al.,
194 2015b). PM_{2.5} was observed by an online PM_{2.5} measuring instrument (METONE, BAM-1020) with a time
195 resolution of 1 hour. Aerosol surface area density was calculated using data from an WPS (wide particle
196 spectrometer, MSP model 1000XP) with a time resolution of 5 min. HCHO was measured with the DNPH method
197 from 19 to 30 December 2015 and the sampling time was 2 hours during the campaign. Detailed operation
198 procedures about the DNPH method in this study can refer to our previous work (Ma et al., 2016). Photolysis

199 frequencies (J values), including J(O¹D), J(NO₂), J(HONO), J(H₂O₂), J(HCHO) and J(NO₃), were calculated based
200 on measurements by an ultra-fast charged coupled device (CCD) detector spectrometer (Meteorology Consult
201 Gmbh, Germany). The acquisition time for J values was 1 min. Other photolysis frequencies (such as carbonyls
202 with more than two carbons) used in the model were calculated by Eq. (2) (Jenkin et al., 1997):

$$203 \quad J_i = L_i \cos(\chi) M_i \exp(-N_i \sec(\chi)) \quad (2)$$

204 where χ is the solar zenith angle; L_i , M_i and N_i are photolysis parameters and are taken from Jenkin et al. (1997),
205 for clear sky conditions. The calculated photolysis frequencies were then scaled by the measured J(NO₂) for
206 cloudiness correction.

207 Volatile organic compounds (VOC) measurements were conducted using a commercial gas chromatograph
208 equipped with a flame ionization detector (GC-FID) (AMA, GC5000). Sixty VOC species including C₂-C₁₂
209 hydrocarbons were detected with a time resolution of 1 hour. Ten of the most reactive alkenes were used in the
210 ozonolysis reaction in the box model simulations. Although the oxygenated VOCs (OVOCs) other than
211 formaldehyde and some other carbonyls (by the DNPH method) were not measured in this study, they were
212 simulated in the box model that was constrained to measured VOCs. Our results indicated that OVOCs only
213 accounted for a small portion of the total VOCs in this industrial area and even contributed much less to the total
214 VOC OH reactivity. Therefore, the limited VOCs detected in this work would not significantly affect the following
215 model simulation results.

216 **2.3 Box Model**

217 To evaluate the effect of HONO on daytime atmospheric oxidation capacity, a chemical box model with the
218 Master Chemical Mechanism (MCMv3.2) (Jenkin et al., 2012) was applied to calculate the concentrations of OH,
219 HO₂ radicals and their production and loss rates using the FACSIMILE software package (UES Software Inc.).
220 Kinetic rate coefficients were taken from the MCM website (<http://mcm.leeds.ac.uk/MCM/>). In this study, the

221 model simulation was constrained with hourly averaged measurement results, including HONO, O₃, NO, NO₂, CO,
222 SO₂, HCHO, VOCs, as well as water vapor, temperature, pressure, and photolysis frequencies.

223 Monte Carlo sensitivity analyses were conducted to assess the model performance. In each Monte Carlo
224 simulation, the input variables of the model, including HONO, O₃, NO, NO₂, CO, SO₂, HCHO, VOCs, reaction
225 rate constants, photolysis frequencies and the planetary boundary layer (PBL) height were independently set to
226 vary within $\pm 10\%$ of the mean value of individual variable with a normal probability distribution.

227

228 **3 Results and Discussion**

229 **3.1 Data Overview**

230 Figure 2 shows the time series of NO, NO₂, O₃, PM_{2.5}, HONO, HCHO, J(HONO) and meteorological
231 parameters, including wind direction, wind speed, temperature and RH. During the entire campaign period, the
232 wind speed ranged from 0.1 to 8.1 m s⁻¹ with an average of 1.7 m s⁻¹. The temperature varied between -4.1 and 16.1
233 °C with an average of 6.1 °C; RH varied from 17 to 96 % with an average of 68 %.

234 During the entire measurement period, the HONO mixing ratios ranged from 0.03 to 7.04 ppbv with a mean
235 value of 1.32 ± 0.92 ppbv. Table 1 lists recent HONO observations conducted in China. Our result was comparable
236 to HONO observed in Xinken (Su et al., 2008) and Beijing (Spataro et al., 2013; Wang et al., 2017) but higher than
237 Xianghe, Beijing (Hendrick et al., 2014), Jinan (Wang et al., 2015a), Hong Kong (Xu et al., 2015) and Shanghai
238 (Wang et al., 2013). Clearly, the general trend of HONO was closely following that of NO₂, which is the dominant
239 precursor of HONO. More markedly, building up of HONO frequently proceeded the accumulations of PM_{2.5}, e.g.,
240 on the 7th and from the 21st - 22nd of December 2015, indicating that HONO may promote the formation of
241 secondary aerosol by contributing to OH production, which will be further analyzed in details in the following

242 sections. The campaign averaged diurnal variations of HONO, NO₂, HONO/NO₂ ratio and aerosol S/V are showed
243 in Fig. 3. HONO started to accumulate after sunset and reached its daily averaged maxima of ~2.0 ppbv at 08:00
244 local time (LT). Later the day, the HONO mixing ratio decreased rapidly due to its fast photolysis and increase of
245 the PBL height. Evidently, daytime HONO was sustained at a relatively high level. The daily averaged minimum
246 of ~0.6 ppbv was observed around 16:00 LT. The mixing ratio of NO₂ varied from 9.5 to 48.7 ppbv with an average
247 of 23.9 ± 7.5 ppbv and a daily averaged maximum of 27.7 ± 8.8 ppbv. NO, O₃ and PM_{2.5} mixing ratios were in the
248 range of 2.7 to 124.9 ppbv, 3 to 39 ppbv and 15 to 345 $\mu\text{g m}^{-3}$, respectively. Meanwhile, the HONO-to-NO₂ ratios
249 ranged from 0.02 to 0.07, with an average of 0.05 ± 0.03 .

250 3.2 OH Simulation

251 Although atmosphere oxidation capacity is determined by the levels of all major oxidants in the atmosphere
252 (e.g., OH, O₃ and NO₃), OH radical is the primary oxidant in the atmosphere and series of reactions initiated by
253 OH radical can lead to the formation of other major secondary oxidants, such as O₃ and NO₃. Fully understanding
254 the budget of OH radical especially the sources of OH radical is of paramount importance for the purpose of
255 controlling the atmosphere oxidation capacity and hence to establish effective air pollution mitigation strategies.

256 *In-situ* measurement of OH radical is often limited by the availability of suitable measurement techniques,
257 which are often suffered from large amount of unresolved uncertainties (Tanner and Eisele, 1995) and the
258 observation often disagree with the modeling results to a large extent. Nevertheless, theoretically some critical
259 parameters to govern the OH radical budget in the atmosphere are difficult to measure directly, such as the
260 formation rates of OH. Accordingly, a box model is often utilized to simulate these highly reactive species to
261 investigate their photochemistry.

262 In order to assess the relative contributions of potential OH sources in this study, we have utilized a box model
263 based on the Master Chemical Mechanism (MCMv3.2) (Jenkin et al., 2012) to simulate the OH concentration and

264 the OH formation rates from various sources. The model simulation was constrained by the measurement results,
 265 including HONO, O₃, NO, NO₂, CO, SO₂, VOCs, as well as water vapor, temperature, pressure and photolysis
 266 frequencies. Since HCHO measurement was only available from 19 to 30 December, simulated HCHO was used
 267 for the entire campaign period. We found that the ratio between simulated to measured HCHO was 1.4 with a
 268 correlation coefficient of R = 0.77. Therefore, we applied a factor of 1.4 to the simulated HCHO in the model to
 269 better represent the HCHO concentration in the atmosphere.

270 The simulated OH time series during the campaign period is shown in Fig. 4. Because the simulation is
 271 constrained by the observations, only within periods when all data are available simulation were conducted.
 272 Simulated OH concentration was in the range of 1.06×10^6 to 5.26×10^6 molecules cm⁻³, similar to the concentration
 273 observed in London (Emmerson et al., 2007), but lower than that measured in New York City (3×10^6 to 3.3×10^7)
 274 (Ren et al., 2003) and Guangzhou (1.5×10^7 to 2.6×10^7) (Lu et al., 2012).

275 It should be noted that the absolute values of the simulated OH may differ from the actual ambient
 276 concentration. However, the general trend of OH evidently followed the solar radiation intensity, indicating its
 277 photochemical production origin. Clearly, the diurnal variation of OH profile is more complicated than that of
 278 photolysis rates because OH production can be affected not only by photochemical processes, but also by both
 279 primary emissions (e.g., HONO and HCHO) and other non-photochemical related heterogeneous processes, such
 280 as HONO production on various surfaces and ozonolysis of alkenes. These processes will be further discussed in
 281 the following sections.

282 3.3 OH Formation Rates

$$283 \quad P_{OH}(HONO)_{net} = J(HONO)[HONO] - k_{OH+NO}[NO][OH] \quad (3)$$

$$284 \quad P_{OH}(O_3) = 2J(O^1D)[O_3]\phi_{OH} \quad (4)$$

$$285 \quad P_{OH}(HCHO) = 2J(HCHO)[HCHO] \quad (5)$$

$$P_{OH}(H_2O_2) = 2J(H_2O_2)[H_2O_2] \quad (6)$$

$$P_{OH}(O_3 + alkenes) = \sum k_{alkene(i)+O_3}[alkene(i)][OH]Y_{OH_i} \quad (7)$$

286
 287
 288 Previous field studies have demonstrated that HONO photolysis can contribute substantially to the OH
 289 production during daytime (Elshorbany et al., 2009; Hendrick et al., 2014; Kleffmann et al., 2005; Su et al., 2008).
 290 In this study, we evaluated the OH formation rates from the photolysis of HONO (Eq. 3), ozone (Eq. 4),
 291 formaldehyde (Eq. 5) and hydrogen peroxide (H₂O₂) (Eq. 6), as well as ozonolysis of alkenes (Eq. 7). The second
 292 term in Eq. 3 is to account for the loss of OH due to the HONO formation from OH + NO, where the OH
 293 concentration was simulated using the box model, so that the net OH formation from the photolysis of HONO is
 294 considered. J values are the photolysis frequencies of the corresponding species and ϕ_{OH} is the fraction of O(¹D)
 295 reacts with H₂O instead of being quenched by nitrogen (N₂) or oxygen (O₂). The OH production by the photolysis
 296 of formaldehyde was calculated assuming that HO₂ formed from reaction R4 was immediately converted into OH
 297 by reaction R8 due to high NO levels in this polluted environment. In Eq. 7, Y_{OH_i} is the yield of OH from gas-
 298 phase reaction of O₃ and alkene(i) and $k_{alkene(i)+O_3}$ is the reaction rate constant for the reaction of O₃ with alkene(i).
 299 The rate constants of the ozonolysis reactions and the corresponding OH yields used in this work are listed in Table
 300 2. Since H₂O₂ was not measured during this campaign, H₂O₂ was estimated from literature values, i.e., 0.5 to 5
 301 ppbv (Guo et al., 2014; Hua et al., 2008; Ren et al., 2009) and a constant of 3 ppbv H₂O₂ was used in this work.

302 The calculated campaign averaged OH production rates from the photolysis of HONO, O₃, HCHO and H₂O₂
 303 along with ozonolysis of alkenes were 7.13×10^6 , 2.46×10^6 , 1.60×10^6 , 2.39×10^5 and 3.94×10^6 molecules cm⁻³ s⁻¹,
 304 respectively, which were comparable with the literature values (Alicke et al., 2002; Chan et al., 2017; Su et al.,
 305 2008). As shown in Fig. 5, the contribution of HONO photolysis to OH production during 7:00-16:00 local time
 306 varied from 23.6 to 63.3% with a mean value of 44.8%. The ozonolysis of ten highly reactive alkenes (listed in
 307 Table 2) by ozone was the second largest contributor to OH radical and the contribution varied from 16.1 to 60.9%
 308 with a mean of 30.3%. The contribution of ozone photolysis was in the range of 1.3 to 24.7% with a mean of 14.9%.

309 The contribution of HCHO photolysis varied between 0.9 and 12.5% with a mean of 8.1%, and the contribution of
310 H₂O₂ photolysis was negligible with an average contribution of 1.9%. The contributions from different OH sources
311 in this study was similar to those found in two wintertime studies. In a study conducted in New York City in winter
312 2004, it was found that 48% of the net HO_x production was from the HONO photolysis, 36% from the ozonolysis
313 of alkenes, only 6% from the HCHO photolysis, and 1% from the O₃ photolysis (Ren et al., 2006). In another study
314 conducted in London in winter 2000, 62% of the OH production was found from the ozonolysis of alkenes, 35%
315 from the HONO photolysis, only 6% from the HCHO photolysis, and <1% from the O₃ photolysis (Heard et al.,
316 2004).

317 The striking features of the Fig. 5 is that HONO photolysis and ozonolysis of alkenes contributed more than
318 70% of the OH production rate on average. In the early morning, HONO photolysis was the dominant source of
319 OH and may boost the photochemistry right after sunrise. As O₃ accumulated, alkene ozonolysis and O₃ photolysis
320 became more and more important. The higher percentage of the HONO photolysis in this study is most likely
321 because of the higher concentrations of HONO observed in the study area and its sources will be further investigated
322 in the following sections.

323 **3.4 Industrial Plumes**

324 Industrial emissions are responsible for a large portion of the haze formation in China. With the
325 implementations of more and more strict mitigation strategies, primary emissions have been reduced substantially
326 in China. However, the observation site was located just ~5 km from the Nanjing industry park, one of the largest
327 industrial zones in the YRD region, which is populated with various heavy industry facilities, including steel mills,
328 power generation stations, and petrochemical refineries. Despite the great effort to reduce primary industrial
329 emissions from these facilities, industrial plumes have often been detected at the site, carrying fair amounts of NH₃,
330 NO_x, SO₂ and VOCs (Ma et al., 2016; Zheng et al., 2015a). To investigate the effects of industrial emissions on

331 local and regional air quality and particularly the role of HONO on the transformation of primary emissions into
332 secondary air pollutants, we have paid special attention into the air masses originated from the industrial zone.
333 Figure 6 depicts the contribution fractions of OH production rates from HONO photolysis, alkene ozonolysis, O₃
334 photolysis, HCHO photolysis and H₂O₂ photolysis during two industrial plume events. The wind rose plots in Fig.
335 6 indicate that the origins of these air masses were all from the nearby industry zone. Unlike that depicted in Fig.
336 5, during the two industry pollution events HONO photolysis along with ozonolysis of alkenes dominated the OH
337 production throughout the day. This was most likely due to the high concentrations of NO_x and VOC within the
338 industrial plumes. More interestingly, the average PM_{2.5} concentrations during the two events were 139 and 239 μg
339 m⁻³, respectively. Evidently, HONO photolysis and ozonolysis may even play a more important role in OH
340 production during severe haze events. Although ambient OH concentrations during these events may not be high
341 (see Fig. 4a), the high levels of HONO can boost active photochemical oxidation and thus promote the formation
342 of other secondary air pollutants.

343 **3.5 HONO Sources**

344 **3.5.1 Primary HONO Emissions**

345 Previous studies have demonstrated that HONO can be emitted directly from vehicle exhaust (Kirchstetter et
346 al., 1996; Kurtenbach et al., 2001). However, the NO/NO_x ratio measured in this work was relatively low, with an
347 average of 0.25±0.06, much less than that of freshly emitted exhausts (> 0.9) obtained from tunnel experiments
348 (Kurtenbach et al., 2001), indicating that the air masses sampled in this work had been considerably aged and mixed
349 with other air masses, and hence primary HONO from direct emissions (if there was any) had been diluted
350 substantially (less than a few per cents) before reaching the observation site. In addition, our sampling site is located
351 nearby the industrial zone, and the high concentration of NO_x was mainly originated from the industrial activities,
352 so the influence of traffic source on HONO was expected to be small. To further evaluate the potential impact of

353 primary emissions on HONO concentration, we have incorporated the contribution of primary HONO emissions
354 into the MCM box model. The HONO emission ratios, i.e., HONO/NO_x, was taken as 0.3% (Kirchstetter et al.,
355 1996), representing a gasoline-fueled vehicle fleet, which was very typically encountered in the study area. On
356 average, the primary emissions from vehicle exhaust can only account for 11% of the total HONO concentration,
357 indicating secondary mechanisms still dominated HONO level in the study area, which will be further analyzed in
358 the following sections.

359 3.5.2 HONO Conversion Rate

360 In addition to primary emission, heterogeneous reactions of NO₂ on surfaces are believed to be the major
361 formation pathways of nocturnal HONO. In order to discuss the influence of secondary mechanisms on HONO,
362 the observed HONO was corrected by removing the portion of primary emission (HONO_{emis}) and was denoted as
363 HONO_{corr} (= HONO - HONO_{emis}).

364 The HONO conversion rate k(het) (hr⁻¹) is an important parameter to compare HONO formation under various
365 NO₂ levels (Xu et al., 2015). In this work, we calculate the HONO conversion rate using the Eq. (8) (Alicke et al.,
366 2003):

$$367 \quad k(\text{het}) = \frac{[\text{HONO}_{\text{corr}}]_{t_2} - [\text{HONO}_{\text{corr}}]_{t_1}}{(t_2 - t_1)[\text{NO}_2]} \quad (8)$$

368 where [HONO_{corr}]_{t₁} and [HONO_{corr}]_{t₂} are the corrected HONO concentrations at two different times, t₁ and t₂,
369 respectively, [NO₂] is the average NO₂ concentration between time t₁ and t₂. The time periods used to calculate
370 HONO/NO₂ conversion ratio were selected when both HONO and NO₂ increased monotonically with a correlation
371 coefficient higher than 0.8. Note Eq. (8) is a simplified demonstration to calculate the reaction rate coefficient of
372 the heterogeneous conversion from NO₂ to HONO at night, which can be dependent on different pollution levels.
373 In this study, the averaged k(het) was determined to be ~0.8% hr⁻¹, which was comparable to the results in the urban
374 sites of Xi'an (0.91% hr⁻¹) (Huang et al., 2017) and Shanghai (0.7% hr⁻¹), China (Wang et al., 2013), but much less

375 than some other observations, such as Back Garden, Guangdong, China ($2.4\% \text{ hr}^{-1}$) (Li et al., 2012), Xinken,
376 Guangdong, China ($1.6\% \text{ hr}^{-1}$) (Li et al., 2012) and Rossfeld, Rhine Valley, France ($2.2\% \text{ hr}^{-1}$) (Acker and Möller,
377 2007). Nevertheless, the high level of NO_x observed in this work may still lead to high level of HONO through
378 various mechanisms.

379 3.5.3 Heterogeneous Conversion of NO_2

380 Previous studies have suggested that heterogeneous conversion of NO_2 on wet surfaces could be an important
381 nocturnal HONO source (Finlayson-Pitts et al., 2003; Wang et al., 2017). However, it appears that the proposed
382 reaction mechanism ($2\text{NO}_2 + \text{H}_2\text{O}$) was limited by the uptake of NO_2 on the wet surfaces (on the order of 10^{-6}) and
383 thus was too slow to account for the observed NO_2 to HONO conversion ratio (Kleffmann et al., 1998). Instead,
384 the reaction between NO_2 and adsorbed semi-volatile organic compounds on soot or aerosol surfaces has been
385 suggested to be one to two orders of magnitudes faster than the aforementioned reaction (George et al., 2005;
386 Gutzwiller et al., 2002) even though the actual reaction mechanism is still under active research. It also should be
387 noted that during nighttime as ambient temperature decreased, the PBL height also decreased, causing the ground
388 surface to air volume ratio to increase, which may also contribute to higher NO_2 to HONO conversion efficiency
389 (Stutz et al., 2004). However, as shown in Fig. 7, $\text{HONO}_{\text{corr}}/\text{NO}_2$ correlated with S/V to some extent and the
390 correlation increased with the product of RH and S/V. Therefore, even though the contribution of HONO formation
391 on the ground surface was present, the aerosol surface was certainly involved in the HONO formation process. The
392 impact of RH on the heterogeneous formation of HONO was further investigated. Figure 8 shows the relationship
393 between $\text{HONO}_{\text{corr}}/\text{NO}_2$ ratio and RH at night. The linearity of the bin points clearly displays the linear correlations
394 between HONO conversion ratio and RH. Following the method introduced by Stutz et al. (2004), we plotted the
395 top-5 values of $\text{HONO}_{\text{corr}}/\text{NO}_2$ ratio (representing steady state conditions) in each 10% RH interval. The conversion
396 efficiency of NO_2 to HONO correlates very well with RH ($R=0.98$), strongly indicating the dependence of HONO

397 formation on RH. Similar phenomenon was also observed at an urban site (Qin et al., 2009) and a rural site (Li et
 398 al., 2012) in Guangzhou, China.

399 3.5.4 Daytime HONO Budget

400 High concentrations of daytime HONO were frequently observed during the campaign period especially
 401 within industrial plumes. If we assume HONO was in photostationary state involving only gas-phase homogeneous
 402 HONO production and photolysis loss, the calculated daytime HONO concentration would be 8.1×10^9 molecules
 403 cm^{-3} , only 24.5% of the observed mean HONO concentration during daytime. Since the gas phase reaction between
 404 OH and NO (i.e., $P_{\text{OH}+\text{NO}}$) and primary emission (i.e., P_{emission}) were unable to explain the observed high HONO
 405 concentrations, daytime HONO budget was further examined in details. Here we designate the unexplained HONO
 406 source as P_{unknown} . The temporal variation of measured HONO concentration can be expressed by the following
 407 equation (Wang et al., 2017):

$$408 \quad \frac{d[\text{HONO}]}{dt} = (P_{\text{OH}+\text{NO}} + P_{\text{emissions}} + P_{\text{unknown}}) - (L_{\text{OH}+\text{HONO}} + L_{\text{photolysis}} + L_{\text{deposition}})$$

409 (9)

410 Thus, P_{unknown} can be calculated as:

$$411 \quad P_{\text{unknown}} = \frac{d[\text{HONO}]}{dt} + L_{\text{OH}+\text{HONO}} + L_{\text{photolysis}} + L_{\text{deposition}} - P_{\text{OH}+\text{NO}} - P_{\text{emission}}$$

$$412 \quad = \frac{d[\text{HONO}]}{dt} + k_{\text{OH}+\text{HONO}}[\text{OH}][\text{HONO}] + J_{\text{HONO}}[\text{HONO}] + \frac{v_{\text{HONO}}}{H}[\text{HONO}]$$

$$413 \quad - k_{\text{OH}+\text{NO}}[\text{OH}][\text{NO}] - \frac{0.003\Delta\text{NO}_x}{\Delta t} \quad (10)$$

414 where $d[\text{HONO}]/dt$ represents the variation of observed HONO concentrations; $L_{\text{photolysis}}$ represents the loss rate of
 415 HONO by photolysis and J_{HONO} is the measured photolysis frequency of HONO; $P_{\text{NO}+\text{OH}}$ and $L_{\text{OH}+\text{HONO}}$ are the gas-
 416 phase formation and loss rates of HONO, respectively; $k_{\text{OH}+\text{NO}}$ and $k_{\text{OH}+\text{HONO}}$ are the corresponding reaction rate
 417 constants; $L_{\text{deposition}}$ is the dry deposition rate of HONO; v_{HONO} represents deposition velocity of HONO and H is
 418 the mixing height; the last term represents direct emissions of HONO. For v_{HONO} , a value of 0.48 cm s^{-1} was

419 adopted (Lee et al., 2016) and the observed mixing height varied from 73 m to 600 m diurnally. A sensitivity
420 analysis with and without the HONO deposition shows that the modeled HONO concentration with HONO
421 deposition loss is 3.5% lower than that without HONO deposition during daytime, indicating that the dry deposition
422 of HONO plays a minor role in HONO losses. The impact of HONO direct emissions was relatively small at
423 daytime. Daytime OH concentration was not measured in this work but was simulated by the MCM box model.

424 Figure 9 shows the average diurnal variation of each individual term in Eq. (10). Compared with $L_{\text{photolysis}}$, the
425 gas-phase reaction between OH and HONO and HONO dry deposition contributed very little to the HONO sink
426 during daytime. However, $P_{\text{OH+NO}}$ and P_{unknown} both contributed significantly to the HONO production and displayed
427 a completely distinct diurnal pattern. Homogeneous reaction between OH and NO reached a maximum of 1.04
428 ppbv hr^{-1} in the early morning (09:00 LT) due to high concentrations of NO in the morning. The unknown source
429 reached a maximum of 1.22 ppbv hr^{-1} around noontime with an average of 0.73 ppbv hr^{-1} , which was about twice
430 as much as averaged $P_{\text{OH+NO}}$. The diurnal profile of P_{unknown} showed a strong photo-enhanced feature, which is
431 consistent with that observed by Michoud et al. (2014) in wintertime Europe.

432 3.5.5 Photo-Enhanced Conversion of NO_2

433 The nature of the unknown source was explored by correlation analyses between P_{unknown} and other HONO
434 production related parameters (see Table 3). P_{unknown} does not correlate well with RH, NO_2 , S/V and J_{NO_2} with the
435 correlation coefficients (R) of 0.27, 0.31, 0.33 and 0.31 respectively. The correlation increased only slightly when
436 heterogeneous conversion of NO_2 ($\text{NO}_2\text{-RH}$, $R = 0.40$) was taken into consideration. It appeared that the unknown
437 HONO sources cannot be well explained by the heterogeneous reactions on wet surfaces alone. Previous studies
438 have suggested that light intensity could be an important parameter influencing the heterogeneous conversion of
439 NO_2 to HONO (Han et al., 2017b; Lee et al., 2016). The photo-enhanced HONO source during the daytime has
440 also been identified in different environments ranging from remote (Villena et al., 2011; Zhou et al., 2002) to urban

441 conditions (Lee et al., 2016). When photo-enhancement was also considered ($J_{\text{NO}_2 \cdot \text{NO}_2 \cdot \text{RH}}$, $R = 0.70$), a
442 significantly better correlation was achieved (Table 3). This suggests that the photosensitized reaction of NO_2 on
443 wet surfaces may be an important source of HONO during daytime. Thus, the improvement in the correlation
444 between HONO and other parameters indicates that photochemistry might indeed play an important role in daytime
445 HONO formation (George et al., 2005; Stemmler et al., 2006). Since the correlation coefficient between P_{unknown}
446 and $J_{\text{NO}_2 \cdot \text{NO}_2 \cdot \text{RH}}$ is comparable with the value between P_{unknown} and $J_{\text{NO}_2 \cdot \text{NO}_2 \cdot \text{S/V} \cdot \text{RH}}$ ($R = 0.70$), either ground or
447 aerosol surfaces can be the dominant reaction site for photosensitized conversion of NO_2 .

448 Since aerosol chemical composition was not measured in this work, we cannot demonstrate any possible direct
449 connection between aerosol composition and the photo-enhanced HONO formation on aerosol surfaces.
450 Nevertheless, the actual mechanism underlying the photo-enhanced HONO formation on aerosol surface needs
451 further investigation. It has been found that photo-sensitized NO_2 conversion rate coefficient on different surfaces
452 can vary substantially (Han et al., 2017a; Stemmler et al., 2006). Furthermore, studies have shown that this type of
453 surface reaction is not catalytic in nature and the surface reaction rate may vary with the availability and aging state
454 of the surface reaction sites (Stemmler et al., 2006). Therefore, aerosol chemical composition alone may not be
455 sufficient to reveal the actual HONO formation processes.

456 **3.5.6 Model Simulation of HONO**

457 The relative contributions of potential HONO sources were assessed by a box model based on the Master
458 Chemical Mechanism (MCMv3.2) (Jenkin et al., 2012). In addition to the homogeneous reaction of NO with OH ,
459 four sources of HONO were included, i.e., heterogeneous HONO formation from NO_2 reaction on aerosol surface
460 and ground surface and light-induced conversion of NO_2 on aerosols and ground surface. Dry deposition of HONO
461 was also considered and a deposition velocity of 0.48 cm s^{-1} was used here (Lee et al., 2016).

462 Most laboratory studies suggest that the heterogeneous reaction on surface leading to HONO is proportional

463 to the first order of NO₂ (Finlayson-Pitts and Pitts, 1999), therefore the HONO formation can be represented by the
 464 following reactions (Li et al., 2010):



467 where k_a and k_g are the first-order rate constants for aerosol and ground surface reactions, respectively. For the
 468 heterogeneous reaction on aerosols, the first order rate constant was estimated as:

$$469 \quad k_a = \frac{\gamma_{\text{NO}_2, \text{aerosol}} \bar{v} (S/V)}{4} \quad (13)$$

470 where \bar{v} is the root mean square (RMS) velocity of NO₂, S/V is the aerosol surface area-to-volume ratio and
 471 $\gamma_{\text{NO}_2, \text{aerosol}}$ is the reactive uptake coefficient on the aerosol surface, with a value of 1×10^{-6} under dark conditions
 472 (Aumont et al., 2003; Li et al., 2010). Under sunlight, however, significant enhancement of NO₂ conversion to
 473 HONO has been found for various types of aerosol surfaces, such as humic acid and similar organic materials
 474 (Stemmler et al., 2007), soot (Monge et al., 2010), and mineral dusts (Ndour et al., 2008). To account for the
 475 photoenhancement, a higher value of uptake coefficient (2×10^{-5}) was used for solar radiation less than 400 W m^{-2}
 476 and an uptake coefficient scaled by (light intensity)/400 for solar radiation larger than 400 W m^{-2} as suggested by
 477 Li et al. (2010). Accordingly, in this work the photoenhanced uptake coefficient was taken as 2×10^{-5} around the
 478 morning hours (~9 AM) and was scaled by the measured photolysis rate of NO₂, i.e., $(J_{\text{NO}_2}) / 2 \times 10^{-3}$ for J_{NO_2} higher
 479 than 2×10^{-3} (the value of J_{NO_2} at ~9 AM).

$$480 \quad k_g = \frac{V_{d, \text{NO}_2}}{2H} \quad (14)$$

$$481 \quad V_{d, \text{NO}_2} = \frac{\gamma_{\text{NO}_2, \text{ground}} \bar{v}}{4.2} \quad (15)$$

482 Equation (14) was used to denote the heterogeneous reactions on the ground surfaces, where V_{d, NO_2} represents
 483 deposition velocity of NO₂; H is the PBL height; and $\gamma_{\text{NO}_2, \text{ground}}$ is the reactive uptake coefficient on the ground.
 484 Here we assume an NO₂ reactive uptake coefficient of 1×10^{-5} (Trick, 2004) in the dark on ground surfaces with a
 485 yield of 50% and increase it to 2×10^{-5} in the daytime, given that the photosensitized reactivity of NO₂ on the ground

486 surface is the same as on the aerosol surface. The observed boundary layer height varied from 73 m to 600 m
487 diurnally. The same scale factor ($(JNO_2)/2 \times 10^{-3}$) was also applied to the daytime ground surface reactions.

488 Figure 10a shows the averaged diurnal profiles of the measured HONO concentration and the simulated
489 HONO concentrations from different sources. In general, the box model can capture the observed HONO trend
490 with very similar magnitude of concentration, with a modeled-to-observed HONO ratio of 1.26 during the day and
491 1.66 at night. In early morning, ground surface appeared to play an important role in HONO heterogeneous
492 production while the PBL was still relatively shallow. However, after ~9:00, despite of the swift developing of PBL,
493 fine particle loading started increasing substantially (as shown in Fig. 3), indicating strong secondary formation of
494 aerosols. Meanwhile, HONO production on aerosol surfaces also increased moderately. We found that higher
495 daytime values were mostly due to the light-induced conversion of NO_2 on aerosol surfaces in addition to the
496 homogeneous reaction of NO with OH. While at night, heterogeneous HONO production on ground surface
497 dominated nocturnal HONO sources and the nighttime aerosol surfaces only contributed slightly (2.2% and 7.9%,
498 respectively) to the total nighttime HONO. The box model tended to under-predict HONO during daytime, which
499 also led to a ~1-hr delay in the peaking time of the simulated HONO. The most likely reason for these disagreements
500 is due to the fact that heterogeneous conversion of NO_2 on various surfaces is too complicated to be fully
501 represented by a single scaling parameter in a linear form. Nevertheless, the general agreement between observation
502 and simulation in this work demonstrated that photo-induced NO_2 conversion on aerosol surfaces was the most
503 important HONO source in the study area during daytime.

504 A Monte Carlo sensitivity analysis was also conducted to assess the model simulation uncertainty of HONO
505 concentration. For each of the 24 hours, 100 independent runs were performed. The Monte Carlo sensitivity
506 analysis show that the model uncertainty of HONO ranged from $\pm 13\%$ to $\pm 38\%$. The sensitivity analysis reinforced
507 the conclusions that the proposed heterogeneous sources can generally capture the observed HONO trend.

508 To investigate the interaction between HONO chemistry and secondary aerosol formations within industrial

509 plumes, we have simulated HONO within the two industrial plume events (see Fig. 6). The results are shown in
510 Fig. 10b. Clearly, HONO was much higher within the industrial plumes comparing to the campaign average (Fig.
511 10a). In addition, we have performed a model sensitivity study with respect to aerosol surface density by varying
512 S/V from 50% to 200% of the average value. The results showed that the contribution from heterogeneous
513 photosensitized conversion of NO₂ on aerosol surfaces would correspondingly vary from 18% to 40% of the total
514 HONO budget, demonstrating that aerosol surface chemistry played an important role during HONO formation in
515 the study area. Indeed, aerosol surfaces were the most important HONO source during daytime (7:00 -16:00 LT),
516 especially in the afternoon. Within the industrial plumes, aerosol surfaces contributed around 35% of the observed
517 daytime HONO and only about 11% of total HONO was from the ground surfaces. The fact that ground surfaces
518 were less important during daytime than nighttime was most likely due to the much higher daytime PBL, causing
519 substantial dilution of HONO formed on the ground surfaces. Meanwhile, secondary particulate matters were
520 rapidly produced within the PBL, providing additional heterogeneous reaction sites for HONO formation as a
521 strong OH source to further promote atmospheric oxidative capacity. It should be noted that the reactive uptake of
522 NO₂ on various surfaces can be highly variable with the type of surfaces. The value used here ($\sim 2 \times 10^{-5}$) is toward
523 the lower end of values reported in the literatures, which is likely the reason that the simulated HONO is generally
524 less than the observations within industrial plumes. The heterogeneous NO₂ uptake kinetics and HONO yields of
525 real atmospheric substrates are still under active study and may be different compared to the artificial surfaces
526 studied in the laboratory setting. Nevertheless, enhanced photosensitized conversion of NO₂ on aerosol surfaces is
527 demonstrated here as a major HONO source in the plumes influenced by industrial emissions.

528

529 4 Conclusions

530 Nitrous acid was measured with a custom-built wet-chemistry based HONO analyzer, together with other
531 atmospheric OH precursors (O_3 and HCHO) at a suburb site of Nanjing in December 2015. The mixing ratios of
532 HONO varied from 0.03 ppbv to 7.04 ppbv with an average of 1.32 ± 0.92 ppbv. Daytime HONO was sustained at
533 a relatively high concentration, with a minimum diurnal hourly average of ~ 0.6 ppbv observed around 16:00 LT. A
534 MCM-box model was used to investigate the HONO chemistry and its impact on atmospheric oxidation capacity
535 in the study area. The results show that the average OH production rates from the photolysis of HONO, ozonolysis
536 of alkenes, photolysis of O_3 , HCHO, and H_2O_2 were 7.13×10^6 , 3.94×10^6 , 2.46×10^6 , 1.60×10^6 and 2.39×10^5
537 molecules $cm^{-3} s^{-1}$, respectively. The box model results show that the average total OH production rate was 1.54×10^7
538 molecules $cm^{-3} s^{-1}$ during daytime, on average about 45% from the photolysis of HONO, 30% from ozonolysis of
539 alkenes, 15% from the photolysis of O_3 , 8% from the photolysis of HCHO and 2% from the photolysis of H_2O_2 .

540 Elevated daytime HONO evidently played an important role in sustaining the atmospheric oxidative capability
541 in the study area, which cannot be explained by the typical OH+NO homogeneous formation mechanism. The
542 observed similarity between the diurnal profiles of HONO/ NO_2 ratio and HONO strongly suggests that HONO was
543 most likely originated from NO_2 heterogeneous reactions. In this study, the averaged NO_2 to HONO conversion
544 rate was determined to be $\sim 0.8\% hr^{-1}$ at night. Good correlation between nocturnal HONO/ NO_2 and the product of
545 $S/V \cdot RH$ supports the heterogeneous NO_2/H_2O reaction mechanism.

546 To fully assess the HONO chemistry in the study area, an MCM box model was developed to examine HONO
547 budget. In general, the box model can capture the observed HONO trend with a modeled-to-observed HONO ratio
548 of 1.26 during the day and 1.66 at night. The model suggests that higher daytime levels of HONO were mainly
549 produced by the light-induced conversion of NO_2 on aerosol surfaces (28.2%) and ground surfaces (17.8%) (except
550 early morning). While the heterogeneous HONO production on ground surface dominated nocturnal HONO

551 sources, heterogeneous reactions on various surfaces only contributed a small portion of total HONO at daytime
552 (2.2% on aerosol surface and 7.9% on ground surface). The box model tends to over-predict HONO at night. The
553 most possible reason for these discrepancies is due to the fact that heterogeneous conversion of NO₂ on various
554 surfaces was too complicated to be fully represented by a single scaling parameter in a linear form. Nevertheless,
555 the general agreement between observation and simulation in this work reiterated that photo-induced NO₂
556 conversion on ground and aerosol surfaces was the most important HONO source in the study area. In the industrial
557 plume case study, it was demonstrated that heterogeneous photosensitized conversion of NO₂ on aerosol surfaces
558 was particularly intensified, when rapid growth of secondary particulate matter was simultaneously observed. Our
559 results indicate that the heterogeneous photosensitized conversion of NO₂ on aerosol surfaces becomes the largest
560 HONO source throughout the daytime, which in turn can enhance OH production, increase the oxidative capacity
561 of atmosphere, and further strengthen the formation of SOA during the daytime in this environment.

562

563 *Author contributions*

564 JZ, YM, and XR designed the experiments, and XS, HJ, YG, WW, YZ, WZ, and YD carried out the field
565 measurements and data analysis. XS and XR performed the MCM box model simulation. JZ, XS, and YM prepared
566 the manuscript with comments from all coauthors.

567 *Acknowledgements*

568 This work was supported by the National Natural Science Foundation of China (Grant numbers 41730106,
569 41575122, 41675126 and 41975172) and the National Key Research and Development Project (Grant number
570 2017YFC0209501). The data used here are listed in the tables, figures, and the supporting materials.

571

572 **References**

573 Acker, K., Möller, D., Wieprecht, W., Meixner, F. X., Bohn, B., Gilge, S., Plass-Dülmer, C., and Berresheim, H.:

- 574 Strong daytime production of OH from HNO₂ at a rural mountain site, *Geophys. Res. Letts.*, 33, L02809,
575 10.1029/2005GL024643, 2006.
- 576 Acker, K., and Möller, D.: Atmospheric variation of nitrous acid at different sites in Europe, *Environ. Chem.*, 4,
577 242-255, <https://doi.org/10.1071/EN07023>, 2007.
- 578 Aliche, B., Platt, U., and Stutz, J.: Impact of nitrous acid photolysis on the total hydroxyl radical budget during the
579 Limitation of Oxidant Production/Pianura Padana Produzione di Ozono study in Milan, *J. Geophys. Res. Atmos.*,
580 107, 8196, 10.1029/2000JD000075, 2002.
- 581 Aliche, B., Geyer, A., Hofzumahaus, A., Holland, F., Konrad, S., Patz, H. W., Schafer, J., Stutz, J., Volz-Thomas,
582 A., and Platt, U.: OH formation by HONO photolysis during the BERLIOZ experiment, *J. Geophys. Res. Atmos.*,
583 108, 17, 8247
584 10.1029/2001jd000579, 2003.
- 585 Ammann, M., Kalberer, M., Jost, D. T., Tobler, L., Rossler, E., Piguet, D., Gaggeler, H. W., and Baltensperger, U.:
586 Heterogeneous production of nitrous acid on soot in polluted air masses, *Nature*, 395, 157-160, 10.1038/25965,
587 1998.
- 588 Atkinson, R., and Arey, J.: Atmospheric degradation of volatile organic compounds, *Chem. Rev.*, 103, 4605-4638,
589 10.1021/cr0206420, 2003.
- 590 Aumont, B., Chervier, F., and Laval, S.: Contribution of HONO sources to the NO_x/HO_x/O₃ chemistry in the
591 polluted boundary layer, *Atmos. Environ.*, 37, 487-498, [https://doi.org/10.1016/S1352-2310\(02\)00920-2](https://doi.org/10.1016/S1352-2310(02)00920-2), 2003.
- 592 Bernard, F., Cazaunau, M., Grosselin, B., Zhou, B., Zheng, J., Liang, P., Zhang, Y., Ye, X., Daele, V., Mu, Y., Zhang,
593 R., Chen, J., and Mellouki, A.: Measurements of nitrous acid (HONO) in urban area of Shanghai, China, *Environ.*
594 *Sci. Pollut. Res. Int.*, 23, 5818-5829, 10.1007/s11356-015-5797-4, 2016.
- 595 Chan, K. L., Wang, S., Liu, C., Zhou, B., Wenig, M. O., and Saiz-Lopez, A.: On the summertime air quality and
596 related photochemical processes in the megacity Shanghai, China, *Sci. Total Environ.*, 580, 974-983,
597 <https://doi.org/10.1016/j.scitotenv.2016.12.052>, 2017.
- 598 Ding, A. J., Fu, C. B., Yang, X. Q., Sun, J. N., Zheng, L. F., Xie, Y. N., Herrmann, E., Nie, W., Petäjä, T., Kerminen,
599 V. M., and Kulmala, M.: Ozone and fine particle in the western Yangtze River Delta: an overview of 1 yr data at
600 the SORPES station, *Atmos. Chem. Phys.*, 13, 5813-5830, 10.5194/acp-13-5813-2013, 2013.
- 601 Elshorbany, Y. F., Kurtenbach, R., Wiesen, P., Lissi, E., Rubio, M., Villena, G., Gramsch, E., Rickard, A. R., Pilling,
602 M. J., and Kleffmann, J.: Oxidation capacity of the city air of Santiago, Chile, *Atmos. Chem. Phys.*, 9, 2257-2273,
603 10.5194/acp-9-2257-2009, 2009.
- 604 Elshorbany, Y. F., Kleffmann, J., Kurtenbach, R., Lissi, E., Rubio, M., Villena, G., Gramsch, E., Rickard, A. R.,
605 Pilling, M. J., and Wiesen, P.: Seasonal dependence of the oxidation capacity of the city of Santiago de Chile,
606 *Atmos. Environ.*, 44, 5383-5394, 10.1016/j.atmosenv.2009.08.036, 2010.
- 607 Elshorbany, Y. F., Steil, B., Brühl, C., and Lelieveld, J.: Impact of HONO on global atmospheric chemistry
608 calculated with an empirical parameterization in the EMAC model, *Atmos. Chem. Phys.*, 12, 9977-10000,
609 10.5194/acp-12-9977-2012, 2012.

610 Emmerson, K. M., Carslaw, N., Carslaw, D. C., Lee, J. D., McFiggans, G., Bloss, W. J., Gravestock, T., Heard, D.
611 E., Hopkins, J., Ingham, T., Pilling, M. J., Smith, S. C., Jacob, M., and Monks, P. S.: Free radical modelling studies
612 during the UK TORCH Campaign in Summer 2003, *Atmos. Chem. Phys.*, 7, 167–181, doi:10.5194/acp-7-167-
613 2007, 2007.

614 Finlayson-Pitts, B. J., and Pitts, J. N.: *Chemistry of the upper and lower atmosphere : theory, experiments and*
615 *applications*, Academic Press, San Diego, Calif., xxii, 969 pp., 1999.

616 Finlayson-Pitts, B. J., Wingen, L. M., Sumner, A. L., Syomin, D., and Ramazan, K. A.: The heterogeneous
617 hydrolysis of NO₂ in laboratory systems and in outdoor and indoor atmospheres: An integrated mechanism, *PCCP*,
618 5, 223-242, 10.1039/b208564j, 2003.

619 Gall, E. T., Griffin, R. J., Steiner, A. L., Dibb, J., Scheuer, E., Gong, L., Rutter, A. P., Cevik, B. K., Kim, S., Lefer,
620 B., and Flynn, J.: Evaluation of nitrous acid sources and sinks in urban outflow, *Atmos. Environ.*, 127, 272-282,
621 10.1016/j.atmosenv.2015.12.044, 2016.

622 George, C., Strekowski, R. S., Kleffmann, J., Stemmler, K., and Ammann, M.: Photoenhanced uptake of gaseous
623 NO₂ on solid organic compounds: a photochemical source of HONO?, *Faraday Discuss.*, 130, 195-210,
624 10.1039/B417888M, 2005.

625 Gerecke, A., Thielmann, A., Gutzwiller, L., and Rossi, M. J.: The chemical kinetics of HONO formation resulting
626 from heterogeneous interaction of NO₂ with flame soot, *Geophys. Res. Letts.*, 25, 2453-2456, 10.1029/98GL01796,
627 1998.

628 Gherman, T., Venables, D. S., Vaughan, S., Orphal, J., and Ruth, A. A.: Incoherent Broadband Cavity-Enhanced
629 Absorption Spectroscopy in the near-Ultraviolet: Application to HONO and NO₂, *Environ. Sci. Technol.*, 42, 890-
630 895, 10.1021/es0716913, 2008.

631 Guo, J., Tilgner, A., Yeung, C., Wang, Z., Louie, P. K. K., Luk, C. W. Y., Xu, Z., Yuan, C., Gao, Y., Poon, S.,
632 Herrmann, H., Lee, S., Lam, K. S., and Wang, T.: Atmospheric Peroxides in a Polluted Subtropical Environment:
633 Seasonal Variation, Sources and Sinks, and Importance of Heterogeneous Processes, *Environ. Sci. Technol.*, 48,
634 1443-1450, 10.1021/es403229x, 2014.

635 Gutzwiller, L., Arens, F., Baltensperger, U., Gäggeler, H. W., and Ammann, M.: Significance of Semivolatile Diesel
636 Exhaust Organics for Secondary HONO Formation, *Environ. Sci. Technol.*, 36, 677-682, 10.1021/es015673b, 2002.

637 Han, C., Liu, Y., and He, H.: Heterogeneous reaction of NO₂ with soot at different relative humidity., *Environ. Sci.*
638 *Pollut. Res.*, 24, 21248–21255, 10.1007/s11356-017-9766-y, 2017a.

639 Han, C., Yang, W., Yang, H., and Xue, X.: Enhanced photochemical conversion of NO₂ to HONO on humic acids
640 in the presence of benzophenone, *Environ. Pollut.*, 231, 979-986, <https://doi.org/10.1016/j.envpol.2017.08.107>,
641 2017b.

642 Heard, D. E., Carpenter, L. J., Creasey, D. J., Hopkins, J. R., Lee, J. D., Lewis, A. C., Pilling, M. J., Seakins, P. W.,
643 Carslaw, N., and Emmerson, K. M.: High levels of the hydroxyl radical in the winter urban troposphere, *Geophys.*
644 *Res. Letts.*, 31, 10.1029/2004gl020544, 2004.

645 Heland, J., Kleffmann, J., Kurtenbach, R., and Wiesen, P.: A New Instrument To Measure Gaseous Nitrous Acid
646 (HONO) in the Atmosphere, *Environ. Sci. Technol.*, 35, 3207-3212, 10.1021/es000303t, 2001.

647 Hendrick, F., Müller, J. F., Clémer, K., Wang, P., De Mazière, M., Fayt, C., Gielen, C., Hermans, C., Ma, J. Z.,
648 Pinardi, G., Stavrakou, T., Vlemmix, T., and Van Roozendaal, M.: Four years of ground-based MAX-DOAS
649 observations of HONO and NO₂ in the Beijing area, *Atmos. Chem. Phys.*, 14, 765-781, 10.5194/acp-14-765-2014,
650 2014.

651 Hofzumahaus, A., Rohrer, F., Lu, K., Bohn, B., Brauers, T., Chang, C. C., Fuchs, H., Holland, F., Kita, K., Kondo,
652 Y., Li, X., Lou, S., Shao, M., Zeng, L., Wahner, A., and Zhang, Y.: Amplified trace gas removal in the troposphere,
653 *Science*, 324, 1702-1704, 10.1126/science.1164566, 2009.

654 Hua, W., Chen, Z. M., Jie, C. Y., Kondo, Y., Hofzumahaus, A., Takegawa, N., Chang, C. C., Lu, K. D., Miyazaki,
655 Y., Kita, K., Wang, H. L., Zhang, Y. H., and Hu, M.: Atmospheric hydrogen peroxide and organic hydroperoxides
656 during PRIDE-PRD'06, China: their concentration, formation mechanism and contribution to secondary aerosols,
657 *Atmos. Chem. Phys.*, 8, 6755-6773, 10.5194/acp-8-6755-2008, 2008.

658 Huang, G., Zhou, X., Deng, G., Qiao, H., and Civerolo, K.: Measurements of atmospheric nitrous acid and nitric
659 acid, *Atmos. Environ.*, 36, 2225-2235, [https://doi.org/10.1016/S1352-2310\(02\)00170-X](https://doi.org/10.1016/S1352-2310(02)00170-X), 2002.

660 Huang, R.-J., Yang, L., Cao, J., Wang, Q., Tie, X., Ho, K.-F., Shen, Z., Zhang, R., Li, G., Zhu, C., Zhang, N., Dai,
661 W., Zhou, J., Liu, S., Chen, Y., Chen, J., and O'Dowd, C. D.: Concentration and sources of atmospheric nitrous acid
662 (HONO) at an urban site in Western China, *Sci. Total Environ.*, 593-594, 165-172,
663 <https://doi.org/10.1016/j.scitotenv.2017.02.166>, 2017.

664 Jenkin, M. E., Saunders, S. M., and Pilling, M. J.: The tropospheric degradation of volatile organic compounds: a
665 protocol for mechanism development, *Atmos. Environ.*, 31, 81-104, [http://dx.doi.org/10.1016/S1352-](http://dx.doi.org/10.1016/S1352-2310(96)00105-7)
666 [2310\(96\)00105-7](http://dx.doi.org/10.1016/S1352-2310(96)00105-7), 1997.

667 Jenkin, M. E., Wyche, K. P., Evans, C. J., Carr, T., Monks, P. S., Alfarra, M. R., Barley, M. H., McFiggans, G. B.,
668 Young, J. C., and Rickard, A. R.: Development and chamber evaluation of the MCM v3.2 degradation scheme for
669 β -caryophyllene, *Atmos. Chem. Phys.*, 12, 5275-5308, 10.5194/acp-12-5275-2012, 2012.

670 Kirchstetter, T. W., Harley, A. R., and Littlejohn, D.: Measurement of nitrous acid in motor vehicle exhaust, *Environ.*
671 *Sci. Technol.*, 30, 2843-2849, 10.1021/es960135y, 1996.

672 Kleffmann, J., Becker, K. H., and Wiesen, P.: Heterogeneous NO₂ conversion processes on acid surfaces: possible
673 atmospheric implications, *Atmos. Environ.*, 32, 2721-2729, [https://doi.org/10.1016/S1352-2310\(98\)00065-X](https://doi.org/10.1016/S1352-2310(98)00065-X),
674 1998.

675 Kleffmann, J., Kurtenbach, R., Lörzer, J., Wiesen, P., Kalthoff, N., Vogel, B., and Vogel, H.: Measured and
676 simulated vertical profiles of nitrous acid-Part I: Field measurements, *Atmos. Environ.*, 37, 2949-2955,
677 10.1016/S1352-2310(03)00242-5, 2003.

678 Kleffmann, J., Gavriloaiei, T., Hofzumahaus, A., Holland, F., Koppmann, R., Rupp, L., Schlosser, E., Siese, M.,
679 and Wahner, A.: Daytime formation of nitrous acid: A major source of OH radicals in a forest, *Geophys. Res. Letts.*,
680 32, L05818, 10.1029/2005GL022524, 2005.

681 Kleffmann, J., Lörzer, J. C., Wiesen, P., Kern, C., Trick, S., Volkamer, R., Rodenas, M., and Wirtz, K.:
682 Intercomparison of the DOAS and LOPAP techniques for the detection of nitrous acid (HONO), *Atmos. Environ.*,
683 40, 3640-3652, <https://doi.org/10.1016/j.atmosenv.2006.03.027>, 2006.

684 Kleffmann, J., and Wiesen, P.: Technical Note: Quantification of interferences of wet chemical HONO LOPAP
685 measurements under simulated polar conditions, *Atmos. Chem. Phys.*, 8, 6813-6822, [https://doi.org/10.5194/acp-](https://doi.org/10.5194/acp-8-6813-2008)
686 [8-6813-2008](https://doi.org/10.5194/acp-8-6813-2008), 2008.

687 Kurtenbach, R., Becker, K. H., Gomes, J. A. G., Kleffmann, J., Lörzer, J. C., Spittler, M., Wiesen, P., Ackermann,
688 R., Geyer, A., and Platt, U.: Investigations of emissions and heterogeneous formation of HONO in a road traffic
689 tunnel, *Atmos. Environ.*, 35, 3385-3394, [https://doi.org/10.1016/S1352-2310\(01\)00138-8](https://doi.org/10.1016/S1352-2310(01)00138-8), 2001.

690 Lee, J. D., Whalley, L. K., Heard, D. E., Stone, D., Dunmore, R. E., Hamilton, J. F., Young, D. E., Allan, J. D.,
691 Laufs, S., and Kleffmann, J.: Detailed budget analysis of HONO in central London reveals a missing daytime
692 source, *Atmos. Chem. Phys.*, 16, 2747-2764, 10.5194/acp-16-2747-2016, 2016.

693 Li, G., Lei, W., Zavala, M., Volkamer, R., Dusanter, S., Stevens, P., and Molina, L. T.: Impacts of HONO sources
694 on the photochemistry in Mexico City during the MCMA-2006/MILAGO Campaign, *Atmos. Chem. Phys.*, 10,
695 6551-6567, 10.5194/acp-10-6551-2010, 2010.

696 Li, X., Brauers, T., Haseler, R., Bohn, B., Fuchs, H., Hofzumahaus, A., Holland, F., Lou, S., Lu, K. D., Rohrer, F.,
697 Hu, M., Zeng, L. M., Zhang, Y. H., Garland, R. M., Su, H., Nowak, A., Wiedensohler, A., Takegawa, N., Shao, M.,
698 and Wahner, A.: Exploring the atmospheric chemistry of nitrous acid (HONO) at a rural site in Southern China,
699 *Atmos. Chem. Phys.*, 12, 1497-1513, 10.5194/acp-12-1497-2012, 2012.

700 Liang, Y., Zha, Q., Wang, W., Cui, L., Lui, K. H., Ho, K. F., Wang, Z., Lee, S.-c., and Wang, T.: Revisiting nitrous
701 acid (HONO) emission from on-road vehicles: A tunnel study with a mixed fleet, *J. Air Waste Manage.*, 67, 797-
702 805, 10.1080/10962247.2017.1293573, 2017.

703 Lu, K. D., Rohrer, F., Holland, F., Fuchs, H., Bohn, B., Brauers, T., Chang, C. C., Häsel, R., Hu, M., Kita, K.,
704 Kondo, Y., Li, X., Lou, S. R., Nehr, S., Shao, M., Zeng, L. M., Wahner, A., Zhang, Y. H., and Hofzumahaus, A.:
705 Observation and modelling of OH and HO₂ concentrations in the Pearl River Delta 2006: a missing OH source in
706 a VOC rich atmosphere, *Atmos. Chem. Phys.*, 12, 1541-1569, 10.5194/acp-12-1541-2012, 2012.

707 Ma, Y., Diao, Y., Zhang, B., Wang, W., Ren, X., Yang, D., Wang, M., Shi, X., and Zheng, J.: Detection of
708 formaldehyde emissions from an industrial zone in the Yangtze River Delta region of China using a proton transfer
709 reaction ion-drift chemical ionization mass spectrometer, *Atmos. Meas. Tech.*, 9, 6101-6116, 10.5194/amt-9-6101-
710 2016, 2016.

711 Makkonen, U., Virkkula, A., Mäntykenttä, J., Hakola, H., Keronen, P., Vakkari, V., and Aalto, P. P.: Semi-
712 continuous gas and inorganic aerosol measurements at a Finnish urban site: comparisons with filters, nitrogen in
713 aerosol and gas phases, and aerosol acidity, *Atmospheric Chemistry and Physics*, 12, 5617-5631, 10.5194/acp-12-
714 5617-2012, 2012.

715 Michoud, V., Colomb, A., Borbon, A., Miet, K., Beekmann, M., Camredon, M., Aumont, B., Perrier, S., Zapf, P.,
716 Siour, G., Ait-Helal, W., Afif, C., Kukui, A., Furger, M., Dupont, J. C., Haefelin, M., and Doussin, J. F.: Study of
717 the unknown HONO daytime source at a European suburban site during the MEGAPOLI summer and winter field
718 campaigns, *Atmospheric Chemistry and Physics*, 14, 2805-2822, 10.5194/acp-14-2805-2014, 2014.

719 Monge, M. E., D'Anna, B., Mazri, L., Giroir-Fendler, A., Ammann, M., Donaldson, D. J., and George, C.: Light
720 changes the atmospheric reactivity of soot, *Proc. Natl. Acad. Sci. USA*, 107, 6605-6609, 10.1073/pnas.0908341107,
721 2010.

722 Müller, M., Anderson, B. E., Beyersdorf, A. J., Crawford, J. H., Diskin, G. S., Eichler, P., Fried, A., Keutsch, F. N.,
723 Mikoviny, T., Thornhill, K. L., Walega, J. G., Weinheimer, A. J., Yang, M., Yokelson, R. J., and Wisthaler, A.: In
724 situ measurements and modeling of reactive trace gases in a small biomass burning plume, *Atmos. Chem. Phys.*,
725 16, 3813-3824, 10.5194/acp-16-3813-2016, 2016.

726 Nakashima, Y., and Kajii, Y.: Determination of nitrous acid emission factors from a gasoline vehicle using a chassis
727 dynamometer combined with incoherent broadband cavity-enhanced absorption spectroscopy, *Sci. Total Environ.*,
728 575, 287-293, <https://doi.org/10.1016/j.scitotenv.2016.10.050>, 2017.

729 Nash, T.: Nitrous acid in the atmosphere and laboratory experiments on its photolysis, *Tellus*, 26, 175-179,
730 10.3402/tellusa.v26i1-2.9768, 1974.

731 Ndour, M., D'Anna, B., George, C., Ka, O., Balkanski, Y., Kleffmann, J., Stemmler, K., and Ammann, M.:
732 Photoenhanced uptake of NO₂ on mineral dust: Laboratory experiments and model simulations, *Geophys. Res.*
733 *Letts.*, 35, L05812, 10.1029/2007gl032006, 2008.

734 Neftel, A., Blatter, A., Hesterberg, R., and Staffelbach, T.: Measurements of concentration gradients of HNO₂ and
735 HNO₃ over a semi-natural ecosystem *Atmos. Environ.*, 30 (17), 3017-3025, 1996.

736 Neuman, J. A., Trainer, M., Brown, S. S., Min, K.-E., Nowak, J. B., Parrish, D. D., Peischl, J., Pollack, I. B.,
737 Roberts, J. M., Ryerson, T. B., and Veres, P. R.: HONO emission and production determined from airborne
738 measurements over the Southeast U.S., *J. Geophys. Res. Atmos.*, 121, 9237–9250, 10.1002/2016JD025197, 2016.

739 Nie, W., Ding, A. J., Xie, Y. N., Xu, Z., Mao, H., Kerminen, V. M., Zheng, L. F., Qi, X. M., Huang, X., Yang, X.
740 Q., Sun, J. N., Herrmann, E., Petaja, T., Kulmala, M., and Fu, C. B.: Influence of biomass burning plumes on
741 HONO chemistry in eastern China, *Atmos. Chem. Phys.*, 15, 1147-1159, 10.5194/acp-15-1147-2015, 2015.

742 Perner, D., and Platt, U.: Detection of nitrous-acid in the atmosphere by differential optical-absorption, *Geophys.*
743 *Res. Letts.*, 6, 917-920, 10.1029/GL006i012p00917, 1979.

744 Pinto, J. P., Dibb, J., Lee, B. H., Rappenglück, B., Wood, E. C., Levy, M., Zhang, R. Y., Lefèr, B., Ren, X. R., Stutz,
745 J., Tsai, C., Ackermann, L., Golovko, J., Herndon, S. C., Oakes, M., Meng, Q. Y., Munger, J. W., Zahniser, M., and
746 Zheng, J.: Intercomparison of field measurements of nitrous acid (HONO) during the SHARP campaign, *J.*
747 *Geophys. Res. Atmos.*, 119, 5583-5601, 10.1002/2013JD020287, 2014.

748 Platt, U., Perner, D., Harris, G. W., Winer, A. M., and Pitts Jr, J. N.: Observations of nitrous acid in an urban
749 atmosphere by differential optical absorption, *Nature*, 285, 312, 10.1038/285312a0, 1980.

750 Qin, M., Xie, P., Su, H., Gu, J., Peng, F., Li, S., Zeng, L., Liu, J., Liu, W., and Zhang, Y.: An observational study of
751 the HONO-NO₂ coupling at an urban site in Guangzhou City, South China, *Atmos. Environ.*, 43, 5731-5742,
752 <https://doi.org/10.1016/j.atmosenv.2009.08.017>, 2009.

753 Rairoux, P., Koch, B., Moller, D., Göritz, G., Warmbier, G., and Czyzewski, A.: Atmospheric traces monitoring
754 applying Cavity Ring-Down Spectroscopy, *Environ. Sci. Pollut. Res.*, Special issue 4, 68-71, 2002.

755 Ren, X., Brune, W. H., Mao, J., Mitchell, M. J., Leshner, R. L., Simpas, J. B., Metcalf, A. R., Schwab, J. J., Li, Y.,
756 Demerjian, K. L., Felton, H. D., Boynton, G., Adams, A., Perry, J., He, Y., Zhou, X., and Hou, J.: Behavior of OH
757 and HO₂ in the winter atmosphere in New York City: Observations and model comparison, *Atmos. Environ.*, 40,
758 S252–S263, 10.1016/j.atmosenv.2005.11.073, 2006.

759 Ren, X., Gao, H., Zhou, X., Crounse, J. D., Wennberg, P. O., Browne, E. C., LaFranchi, B. W., Cohen, R. C., McKay,
760 M., Goldstein, A. H., and Mao, J.: Measurement of atmospheric nitrous acid at Blodgett Forest during
761 BEARPEX2007, *Atmos. Chem. Phys.*, 10, 6283-6294, 10.5194/acp-10-6283-2010, 2010.

762 Ren, X. R., Harder, H., Martinez, M., Leshner, R. L., Oligier, A., Simpas, J. B., Brune, W. H., Schwab, J. J., Demerjian,
763 K. L., He, Y., Zhou, X. L., and Gao, H. G.: OH and HO₂ chemistry in the urban atmosphere of New York City,
764 *Atmos. Environ.*, 37, 3639-3651, 10.1016/s1352-2310(03)00459-x, 2003.

765 Ren, Y., Ding, A., Wang, T., Shen, X., Guo, J., Zhang, J., Wang, Y., Xu, P., Wang, X., and Gao, J.: Measurement of
766 gas-phase total peroxides at the summit of Mount Tai in China, *Atmospheric Environment*, 43, 1702-1711,
767 10.1016/j.atmosenv.2008.12.020, 2009.

768 Rickard, A. R., Johnson, D., McGill, C. D., and Marston, G.: OH Yields in the Gas-Phase Reactions of Ozone with
769 Alkenes, *The Journal of Physical Chemistry A*, 103, 7656-7664, 10.1021/jp9916992, 1999.

770 Rondon, A., and Sanhueza, E.: High HONO atmospheric concentrations during vegetation burning in the tropical
771 savannah, *Tellus B: Chem. Phys. Meteor.*, 41, 474-477, 10.3402/tellusb.v41i4.15102, 1989.

772 Salmon, O. E., Shepson, P. B., Ren, X., He, H., Hall, D. L., Dickerson, R. R., Stirm, B. H., Brown, S. S., Fibiger,
773 D. L., McDuffie, E. E., Campos, T. L., Gurney, K. R., and Thornton, J. A.: Top-Down Estimates of NO_x and CO
774 Emissions From Washington, D.C.-Baltimore During the WINTER Campaign, *J. Geophys. Res. Atmos.*, 123,
775 7705-7724, 10.1029/2018jd028539, 2018.

776 Scharko, N. K., Martin, E. T., Losovyj, Y., Peters, D. G., and Raff, J. D.: Evidence for Quinone Redox Chemistry
777 Mediating Daytime and Nighttime NO₂-to-HONO Conversion on Soil Surfaces, *Environ. Sci. Technol.*, 51, 9633-
778 9643, 10.1021/acs.est.7b01363, 2017.

779 Sörgel, M., Trebs, I., Wu, D., and Held, A.: A comparison of measured HONO uptake and release with calculated
780 source strengths in a heterogeneous forest environment, *Atmospheric Chemistry and Physics*, 15, 9237-9251,
781 10.5194/acp-15-9237-2015, 2015.

782 Spataro, F., Ianniello, A., Esposito, G., Allegrini, I., Zhu, T., and Hu, M.: Occurrence of atmospheric nitrous acid
783 in the urban area of Beijing (China), *Sci. Total Environ.*, 447, 210-224,
784 <https://doi.org/10.1016/j.scitotenv.2012.12.065>, 2013.

785 Stemmler, K., Ammann, M., Donders, C., Kleffmann, J., and George, C.: Photosensitized reduction of nitrogen
786 dioxide on humic acid as a source of nitrous acid, *Nature*, 440, 195-198, 10.1038/nature04603, 2006.

787 Stemmler, K., Ndour, M., Elshorbany, Y., Kleffmann, J., D'Anna, B., George, C., Bohn, B., and Ammann, M.: Light
788 induced conversion of nitrogen dioxide into nitrous acid on submicron humic acid aerosol, *Atmos. Chem. Phys.*, 7,
789 4237-4248, 10.5194/acp-7-4237-2007, 2007.

790 Stutz, J., Alicke, B., Ackermann, R., Geyer, A., Wang, S. H., White, A. B., Williams, E. J., Spicer, C. W., and Fast,
791 J. D.: Relative humidity dependence of HONO chemistry in urban areas, *J. Geophys. Res. Atmos.*, 109, D03307,
792 doi:10.1029/2003jd004135, 2004.

793 Su, H., Cheng, Y. F., Shao, M., Gao, D. F., Yu, Z. Y., Zeng, L. M., Slanina, J., Zhang, Y. H., and Wiedensohler, A.:
794 Nitrous acid (HONO) and its daytime sources at a rural site during the 2004 PRIDE-PRD experiment in China, *J.*
795 *Geophys. Res. Atmos.*, 113, D14312, 10.1029/2007JD009060, 2008.

796 Su, H., Cheng, Y., Oswald, R., Behrendt, T., Trebs, I., Meixner, F. X., Andreae, M. O., Cheng, P., Zhang, Y., and
797 Poschl, U.: Soil nitrite as a source of atmospheric HONO and OH radicals, *Science*, 333, 1616-1618,
798 10.1126/science.1207687, 2011.

799 Tang, Y., An, J., Wang, F., Li, Y., Qu, Y., Chen, Y., and Lin, J.: Impacts of an unknown daytime HONO source on
800 the mixing ratio and budget of HONO, and hydroxyl, hydroperoxyl, and organic peroxy radicals, in the coastal
801 regions of China, *Atmos. Chem. Phys.*, 15, 9381-9398, 10.5194/acp-15-9381-2015, 2015.

802 Tanner, D. J., and Eisele, F. L.: Present oh measurement limits and associated uncertainties, *J. Geophys. Res. Atmos.*,
803 100, 2883-2892, 1995.

804 Trick, S.: Formation of nitrous acid on urban surfaces - a physicalchemical perspective, Ph.D. thesis, University of
805 Heidelberg, 2004.

806 Trinh, H. T., Imanishi, K., Morikawa, T., Hagino, H., and Takenaka, N.: Gaseous nitrous acid (HONO) and nitrogen
807 oxides (NO_x) emission from gasoline and diesel vehicles under real-world driving test cycles, *J. Air Waste Manage.*,
808 67, 412-420, 10.1080/10962247.2016.1240726, 2017.

809 VandenBoer, T. C., Brown, S. S., Murphy, J. G., Keene, W. C., Young, C. J., Pszenny, A. A. P., Kim, S., Warneke,
810 C., de Gouw, J. A., Maben, J. R., Wagner, N. L., Riedel, T. P., Thornton, J. A., Wolfe, D. E., Dubé, W. P., Öztürk,
811 F., Brock, C. A., Grossberg, N., Lefer, B., Lerner, B., Middlebrook, A. M., and Roberts, J. M.: Understanding the
812 role of the ground surface in HONO vertical structure: High resolution vertical profiles during NACHTT-11, *J.*
813 *Geophys. Res. Atmos.*, 118, 10,155-110,171, 10.1002/jgrd.50721, 2013.

814 Vecera, Z., and Dasgupta, P. K.: Measurement of ambient nitrous acid and a reliable calibration source for gaseous
815 nitrous acid, *Environ. Sci. Technol.*, 25, 255-260, 10.1021/es00014a006, 1991.

816 Villena, G., Kleffmann, J., Kurtenbach, R., Wiesen, P., Lissi, E., Rubio, M. A., Croxatto, G., and Rappenglück, B.:
817 Vertical gradients of HONO, NO_x and O₃ in Santiago de Chile, *Atmos. Environ.*, 45, 3867-3873,
818 10.1016/j.atmosenv.2011.01.073, 2011.

819 Villena, G., Bejan, I., Kurtenbach, R., Wiesen, P., and Kleffmann, J.: Interferences of commercial NO₂ instruments
820 in the urban atmosphere and in a smog chamber, *Atmos. Meas. Tech.*, 5, 149-159, 10.5194/amt-5-149-2012, 2012.

821 Wall, K. J., and Harris, G. W.: Uptake of nitrogen dioxide (NO₂) on acidic aqueous humic acid (HA) solutions as a
822 missing daytime nitrous acid (HONO) surface source, *J. Atmos. Chem.*, 74, 283-321, 10.1007/s10874-016-9342-
823 8, 2016.

824 Wang, J., Zhang, X., Guo, J., Wang, Z., and Zhang, M.: Observation of nitrous acid (HONO) in Beijing, China:
825 Seasonal variation, nocturnal formation and daytime budget, *Sci. Total Environ.*, 587-588, 350-359,
826 <https://doi.org/10.1016/j.scitotenv.2017.02.159>, 2017.

827 Wang, L., Wen, L., Xu, C., Chen, J., Wang, X., Yang, L., Wang, W., Yang, X., Sui, X., Yao, L., and Zhang, Q.:
828 HONO and its potential source particulate nitrite at an urban site in North China during the cold season, *The Science*
829 *of the total environment*, 538, 93-101, 10.1016/j.scitotenv.2015.08.032, 2015a.

830 Wang, M., Chen, W. T., Shao, M., Lu, S. H., Zeng, L. M., and Hu, M.: Investigation of carbonyl compound sources
831 at a rural site in the Yangtze River Delta region of China, *Journal of Environmental Sciences-China*, 28, 128-136,
832 10.1016/j.jes.2014.12.001, 2015b.

833 Wang, S., Zhou, R., Zhao, H., Wang, Z., Chen, L., and Zhou, B.: Long-term observation of atmospheric nitrous
834 acid (HONO) and its implication to local NO₂ levels in Shanghai, China, *Atmos. Environ.*, 77, 718-724,
835 <https://doi.org/10.1016/j.atmosenv.2013.05.071>, 2013.

836 Wong, K. W., Oh, H. J., Lefer, B. L., Rappenglück, B., and Stutz, J.: Vertical profiles of nitrous acid in the nocturnal
837 urban atmosphere of Houston, TX, *Atmos. Chem. Phys.*, 11, 3595-3609, 10.5194/acp-11-3595-2011, 2011.

838 Wong, K. W., Tsai, C., Lefer, B., Haman, C., Grossberg, N., Brune, W. H., Ren, X., Luke, W., and Stutz, J.: Daytime
839 HONO vertical gradients during SHARP 2009 in Houston, TX, *Atmospheric Chemistry and Physics*, 12, 635-652,
840 10.5194/acp-12-635-2012, 2012.

841 Wong, K. W., Tsai, C., Lefer, B., Grossberg, N., and Stutz, J.: Modeling of daytime HONO vertical gradients during
842 SHARP 2009, *Atmos. Chem. Phys.*, 13, 3587-3601, 10.5194/acp-13-3587-2013, 2013.

843 Xu, Z., Wang, T., Wu, J., Xue, L., Chan, J., Zha, Q., Zhou, S., Louie, P. K. K., and Luk, C. W. Y.: Nitrous acid
844 (HONO) in a polluted subtropical atmosphere: Seasonal variability, direct vehicle emissions and heterogeneous
845 production at ground surface, *Atmos. Environ.*, 106, 100-109, <http://dx.doi.org/10.1016/j.atmosenv.2015.01.061>,
846 2015.

847 Xue, L., Gu, R., Wang, T., Wang, X., Saunders, S., Blake, D., Louie, P. K. K., Luk, C. W. Y., Simpson, I., Xu, Z.,
848 Wang, Z., Gao, Y., Lee, S., Mellouki, A., and Wang, W.: Oxidative capacity and radical chemistry in the polluted
849 atmosphere of Hong Kong and Pearl River Delta region: analysis of a severe photochemical smog episode,
850 *Atmospheric Chemistry and Physics*, 16, 9891-9903, 10.5194/acp-16-9891-2016, 2016.

851 Ye, C., Zhou, X., Pu, D., Stutz, J., Festa, J., Spolaor, M., Tsai, C., Cantrell, C., Mauldin, R. L., Campos, T.,
852 Weinheimer, A., Hornbrook, R. S., Apel, E. C., Guenther, A., Kaser, L., Yuan, B., Karl, T., Haggerty, J., Hall, S.,
853 Ullmann, K., Smith, J. N., Ortega, J., and Knote, C.: Rapid cycling of reactive nitrogen in the marine boundary
854 layer, *Nature*, 532, 489-491, 10.1038/nature17195, 2016.

855 Ye, C., Zhang, N., Gao, H., and Zhou, X.: Photolysis of Particulate Nitrate as a Source of HONO and NO_x, *Environ.*
856 *Sci. Technol.*, 51, 6849-6856, 10.1021/acs.est.7b00387, 2017.

857 Zhang, N., Zhou, X., Shepson, P. B., Gao, H., Alaghmand, M., and Stirm, B.: Aircraft measurement of HONO
858 vertical profiles over a forested region, *Geophys. Res. Letts.*, 36, L15820, 10.1029/2009gl038999, 2009.

859 Zheng, J., Ma, Y., Chen, M., Zhang, Q., Wang, L., Khalizov, A. F., Yao, L., Wang, Z., Wang, X., and Chen, L.:
860 Measurement of atmospheric amines and ammonia using the high resolution time-of-flight chemical ionization
861 mass spectrometry, *Atmos. Environ.*, 102, 249-259, <http://dx.doi.org/10.1016/j.atmosenv.2014.12.002>, 2015a.

862 Zheng, J., Ma, Y., Chen, M., Zhang, Q., Wang, L., Khalizov, A. F., Yao, L., Wang, Z., Wang, X., and Chen, L.:
863 Measurement of atmospheric amines and ammonia using the high resolution time-of-flight chemical ionization
864 mass spectrometry, *Atmospheric Environment*, 102, 249-259, 10.1016/j.atmosenv.2014.12.002, 2015b.

865 Zhou, X., Civerolo, K., Dai, H., Huang, G., Schwab, J., and Demerjian, K.: Summertime nitrous acid chemistry in
866 the atmospheric boundary layer at a rural site in New York State, *J. Geophys. Res. Atmos.*, 107, ACH 13-11-ACH
867 13-11, 10.1029/2001jd001539, 2002.

868 Zhou, X., Gao, H., He, Y., Huang, G., Bertman, S. B., Civerolo, K., and Schwab, J.: Nitric acid photolysis on
869 surfaces in low-NO_x environments: Significant atmospheric implications, *Geophys. Res. Letts.*, 30, 2217,

870 10.1029/2003gl018620, 2003.

871 Zhou, X., Zhang, N., TerAvest, M., Tang, D., Hou, J., Bertman, S., Alaghmand, M., Shepson, P. B., Carroll, M. A.,
872 Griffith, S., Dusanter, S., and Stevens, P. S.: Nitric acid photolysis on forest canopy surface as a source for
873 tropospheric nitrous acid, *Nat. Geosci.*, 4, 440-443, 10.1038/ngeo1164, 2011.

874 Ziemba, L. D., Dibb, J. E., Griffin, R. J., Anderson, C. H., Whitlow, S. I., Lefer, B. L., Rappenglück, B., and Flynn,
875 J.: Heterogeneous conversion of nitric acid to nitrous acid on the surface of primary organic aerosol in an urban
876 atmosphere, *Atmos. Environ.*, 44, 4081-4089, 10.1016/j.atmosenv.2008.12.024, 2010.

877

878

879 **Table 1.** Overview on HONO measurements performed in Nanjing and other cities in China.

Location	Date	HONO (ppbv)[#]	References
Beijing	Sep. - Oct. 2015 (autumn)	2.27 ± 1.82	Wang et al. (2017)
	Jan. 2016 (winter)	1.05 ± 0.89	
	Apr. - May 2016 (spring)	1.05 ± 0.95	
	Jun. - Jul. 2016 (summer)	1.38 ± 0.90	
Xi'an	Jul. - Aug. 2015 (summer)	1.12 ± 0.97	Huang et al. (2017)
Jinan	Nov. 2013 - Jan. 2014 (winter)	0.35 ± 0.5	Wang et al. (2015a)
Nanjing	Apr. - Jun. 2012 (spring)	0.76 ± 0.79	Nie et al. (2015)
Xianghe	Mar 2010 - Dec 2012	$0.33 \pm 0.16^*$	Hendrick et al. (2014)
Beijing	Jan. - Feb. 2007(winter)	1.04 ± 0.73	Spataro et al. (2013)
Guangzhou	Jul. 2006 (summer)	$0.71\sim 8.43 (2.8)^{**}$	Qin et al. (2009)
Xinken	Oct. - Nov. 2004 (autumn)	$0.4\sim 3.8 (1.2)^{**}$	Li et al. (2012)
Nanjing	Dec. 2015 (winter)	1.32 ± 0.92	This work

880 [#] Campaign averaged; * Yearly average; ** Only range and mean values are reported

881

882 **Table 2.** Ozonolysis reaction rate constants and OH formation yields of the volatile organic compounds (VOC)
883 used in the calculation.

VOC	$k(298\text{K}) \times 10^{-18}$ ($\text{cm}^3\text{molecule}^{-1}\text{s}^{-1}$) ^a	OH yield	VOC	$k(298\text{K}) \times 10^{-18}$ ($\text{cm}^3\text{molecule}^{-1}\text{s}^{-1}$) ^a	OH yield
Ethene	1.6	0.13 ^b	trans-2-Pentene	160	0.47 ^c
Propene	10.1	0.34 ^b	cis-2-Pentene	130	0.3 ^c
trans-2-Butene	190	0.59 ^b	1-Pentene	10.6	0.37 ^b
cis-2-Butene	125	0.37 ^b	Isoprene	12.8 ^c	0.13 ± 0.03 ^c
1-Butene	9.64	0.41 ^b	Styrene	17	0.07 ^c

884 a: Atkinson and Arey (2003); b: Rickard et al. (1999); c: Alicke et al. (2002)

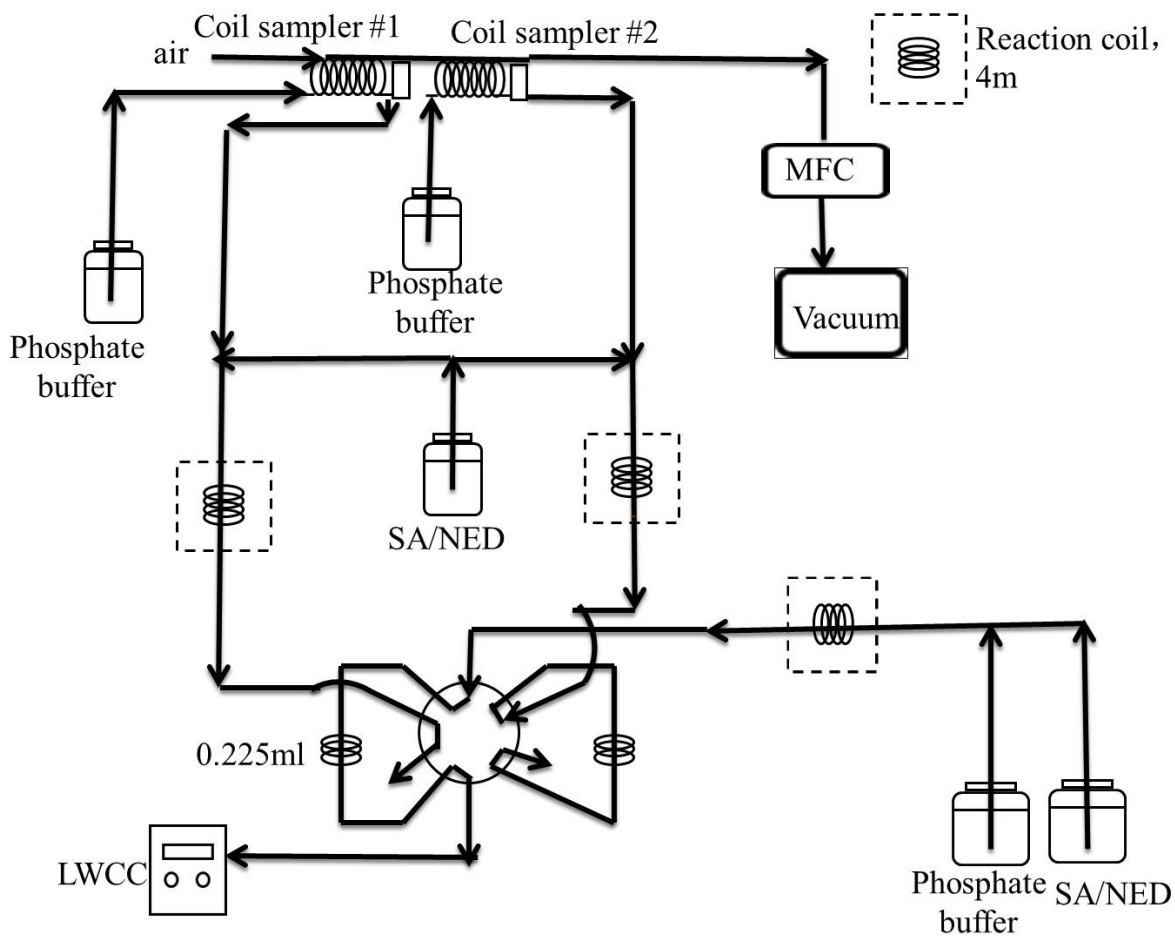
885

886 **Table 3.** Linear correlation coefficients (Pearson correlation, R) of the unknown source to HONO production-
 887 related parameters.

Individual	Correlation Coefficient (R)	Various Combinations of	Correlation Coefficient (R)
RH	0.27	$J(\text{NO}_2) \cdot \text{S/V}$	0.59
NO_2	0.31	$J(\text{NO}_2) \cdot \text{NO}_2$	0.51
S/V	0.33	$J(\text{NO}_2) \cdot \text{RH}$	0.59
$J(\text{NO}_2)$	0.31	$J(\text{NO}_2) \cdot \text{NO}_2 \cdot \text{RH}$	0.70
$\text{NO}_2 \cdot \text{S/V}$	0.36	$J(\text{NO}_2) \cdot \text{NO}_2 \cdot \text{S/V}$	0.61
$\text{NO}_2 \cdot \text{RH}$	0.40	$\text{NO}_2 \cdot \text{RH} \cdot \text{S/V}$	0.44
$\text{RH} \cdot \text{S/V}$	0.39	$J(\text{NO}_2) \cdot \text{NO}_2 \cdot \text{S/V} \cdot \text{RH}$	0.70

888

889

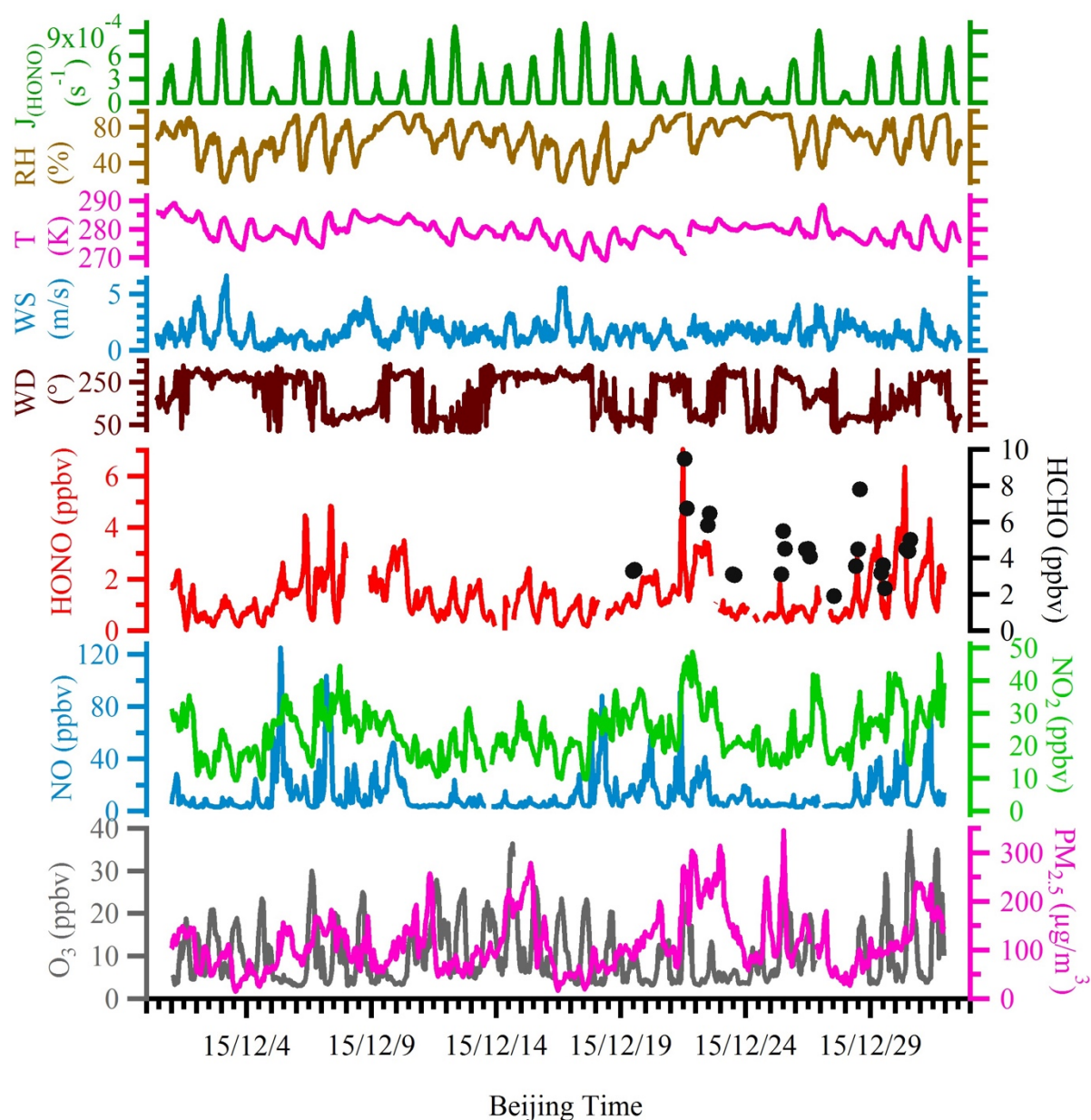


890

891

Figure 1. Schematics of the custom-built wet chemistry-based HONO instrument.

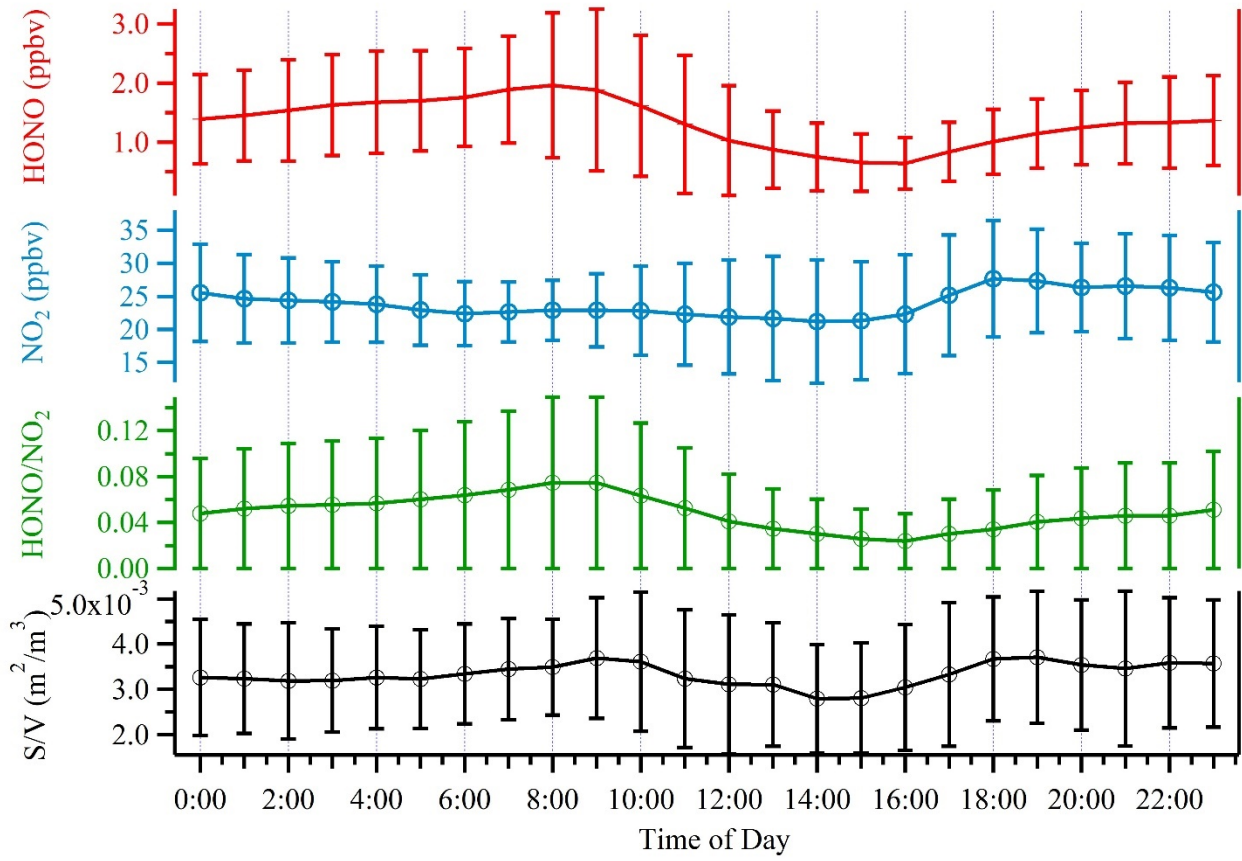
892



893

894 **Figure 2.** Time series of meteorological parameters, including HONO photolysis frequency ($J(\text{HONO})$), relative
 895 humidity (RH), ambient temperature, wind speed and wind direction, as well as mixing ratios of measured HONO,
 896 HCHO, NO, NO₂, O₃ and PM_{2.5} during the observation period.

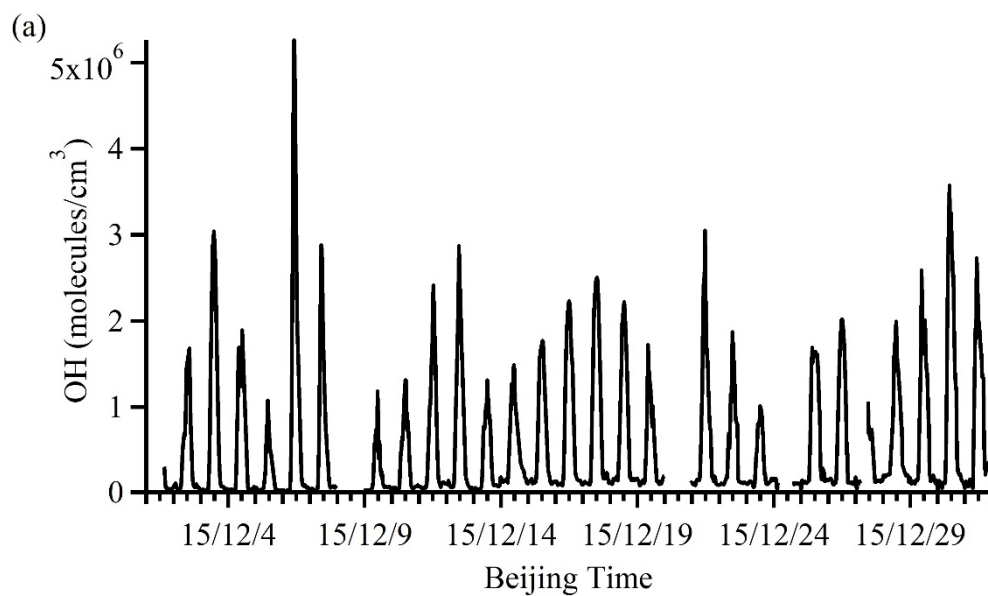
897



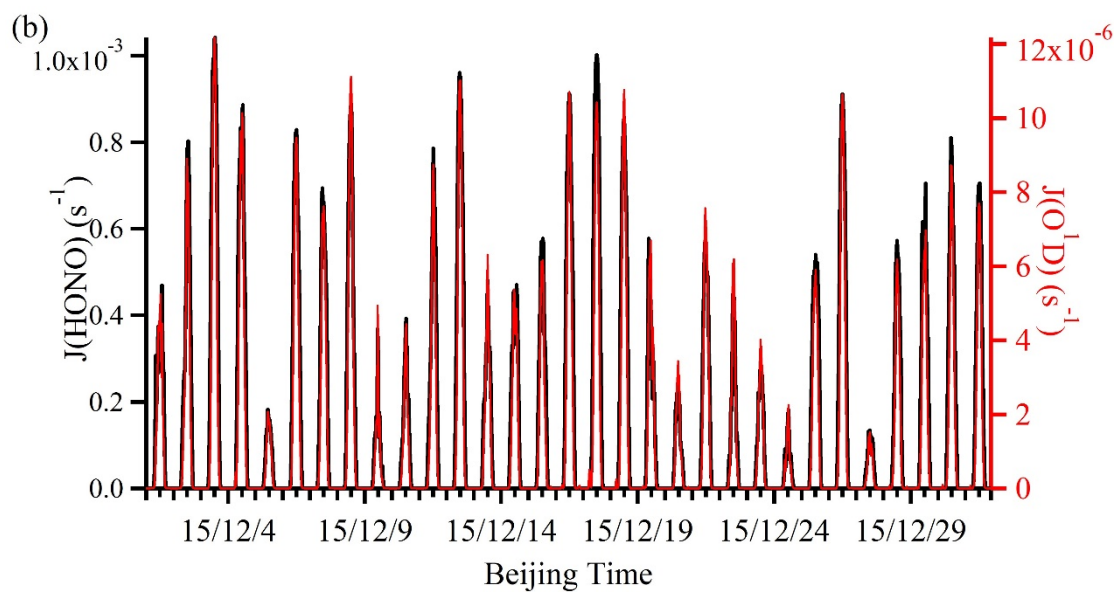
899

900 **Figure 3.** Average diurnal profiles of HONO, NO₂, HONO/NO₂ and S/V. Error bars represent the standard
 901 deviations in hourly bins.

902



903

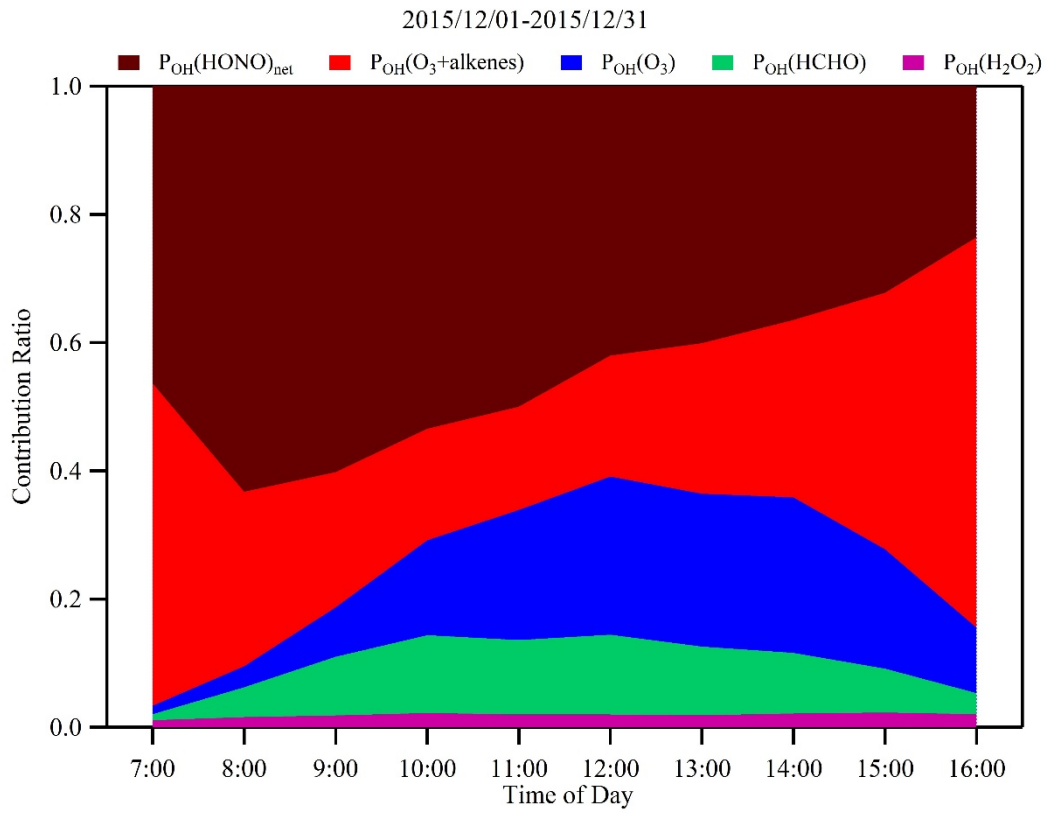


904

905 **Figure 4.** Time series of simulated OH (panel a) and observed photolysis rates (J(HONO) and J(O¹D)) (panel b).

906 The gaps in the OH time series were the time periods when some observation data were not available.

907



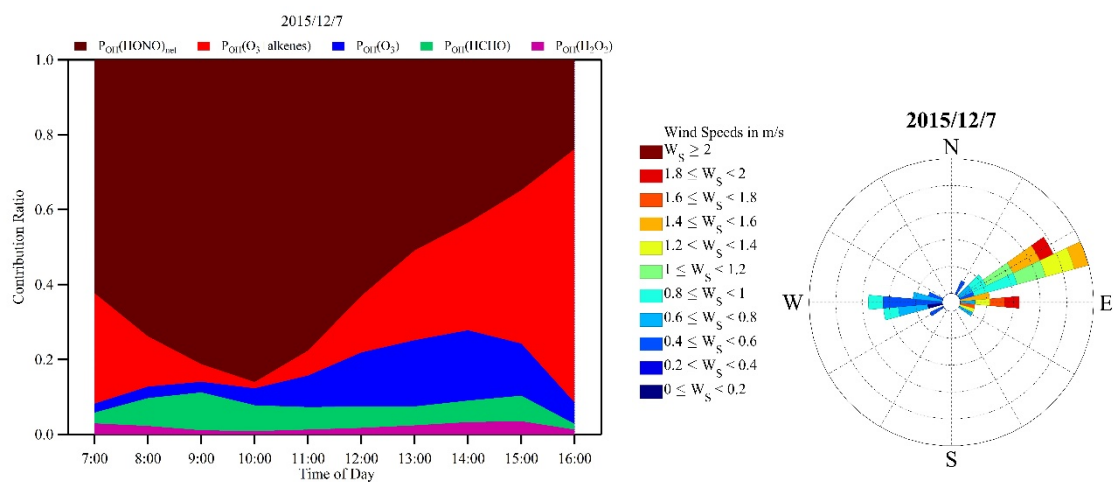
908

909 **Figure 5.** Campaign averaged diurnal variations of contribution fractions of OH production rates from HONO

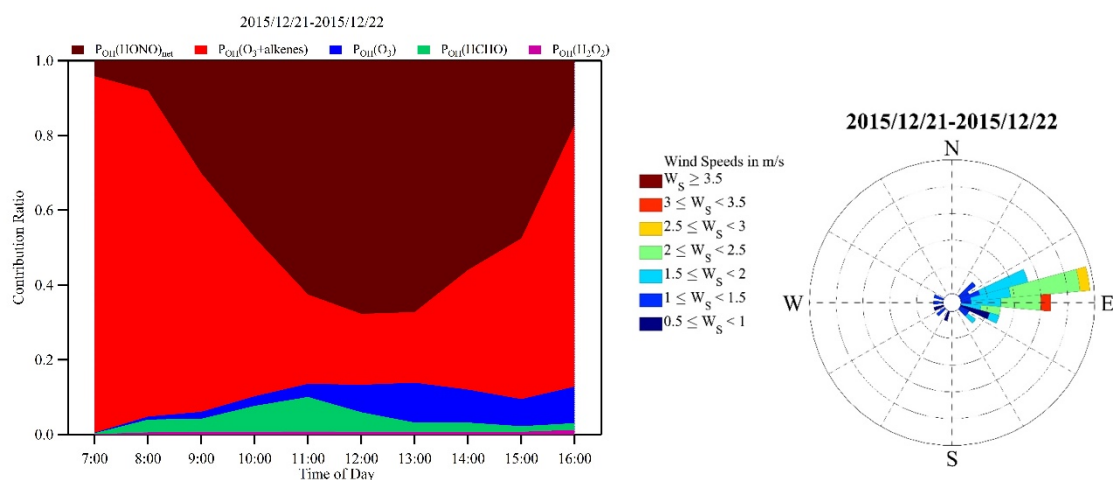
910 photolysis (brown), alkene ozonolysis (red), O₃ photolysis (blue), HCHO photolysis (green) and H₂O₂ photolysis

911 (purple).

912



914



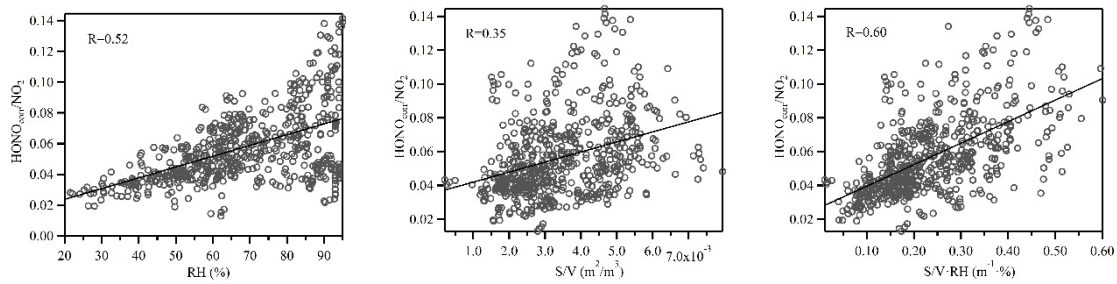
915

916

917 **Figure 6.** The same plots as Fig. 5 during two industrial plume events on the 7th (upper panel) and from the 21st-
 918 22nd (lower panel) of December 2015. The corresponding wind rose plots indicate the origin of these plumes, i.e.,
 919 the industry park to the east of the observation site.

920

921

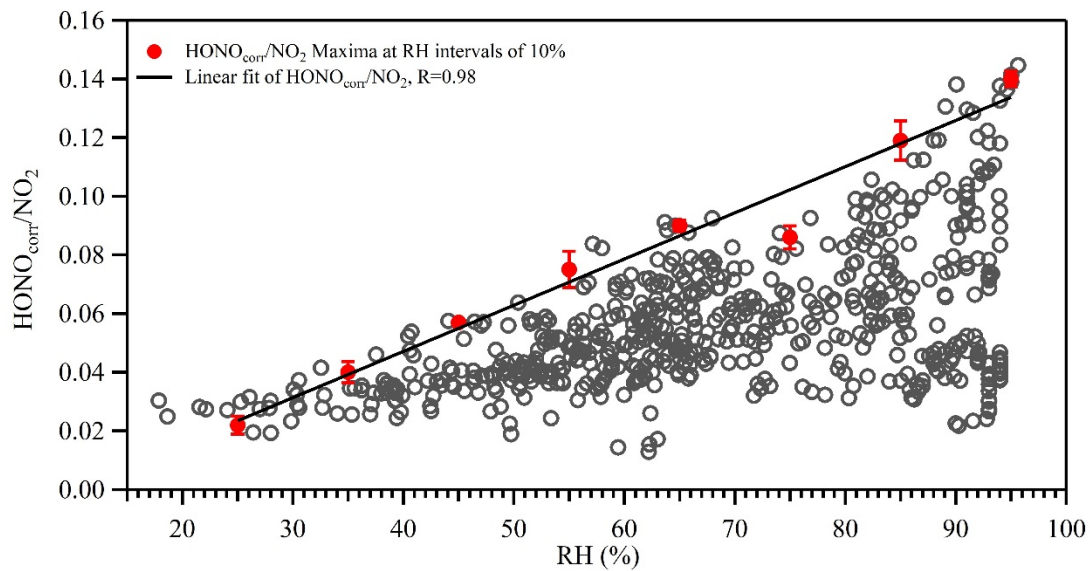


922

923

Figure 7. Nighttime correlations between HONO/NO₂ and RH, S/V and the product of S/V·RH.

924



925

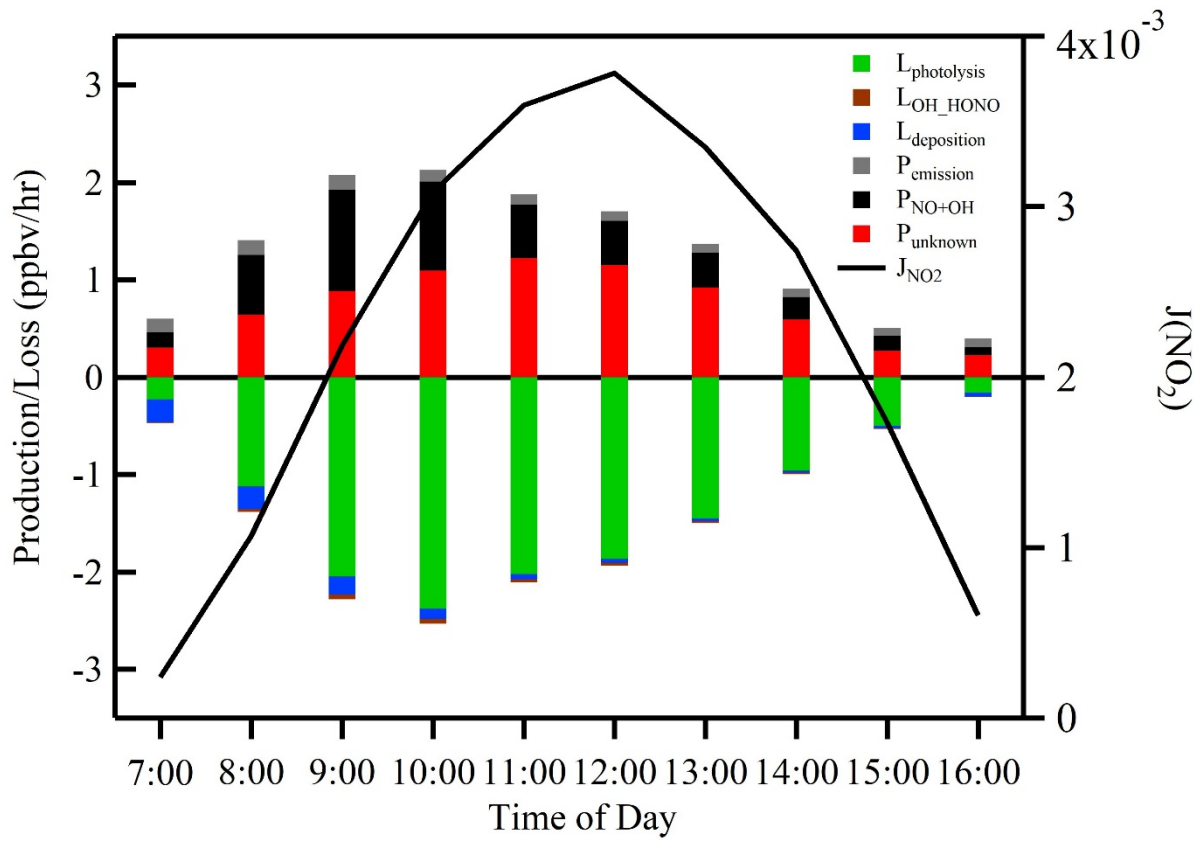
926 **Figure 8.** Correlation between HONO/NO₂ and relative humidity (RH) at night. The open gray circles are 30-min

927 averages. The red circles represent the averages of the top-5 maxima of HONO/NO₂ ratios in 10% RH bins. Error

928 bars represent standard deviations of the top-5 HONO/NO₂ ratios in 10% RH bins. The black line is the linear fit

929 of the red circles for HONO/NO₂ with RH.

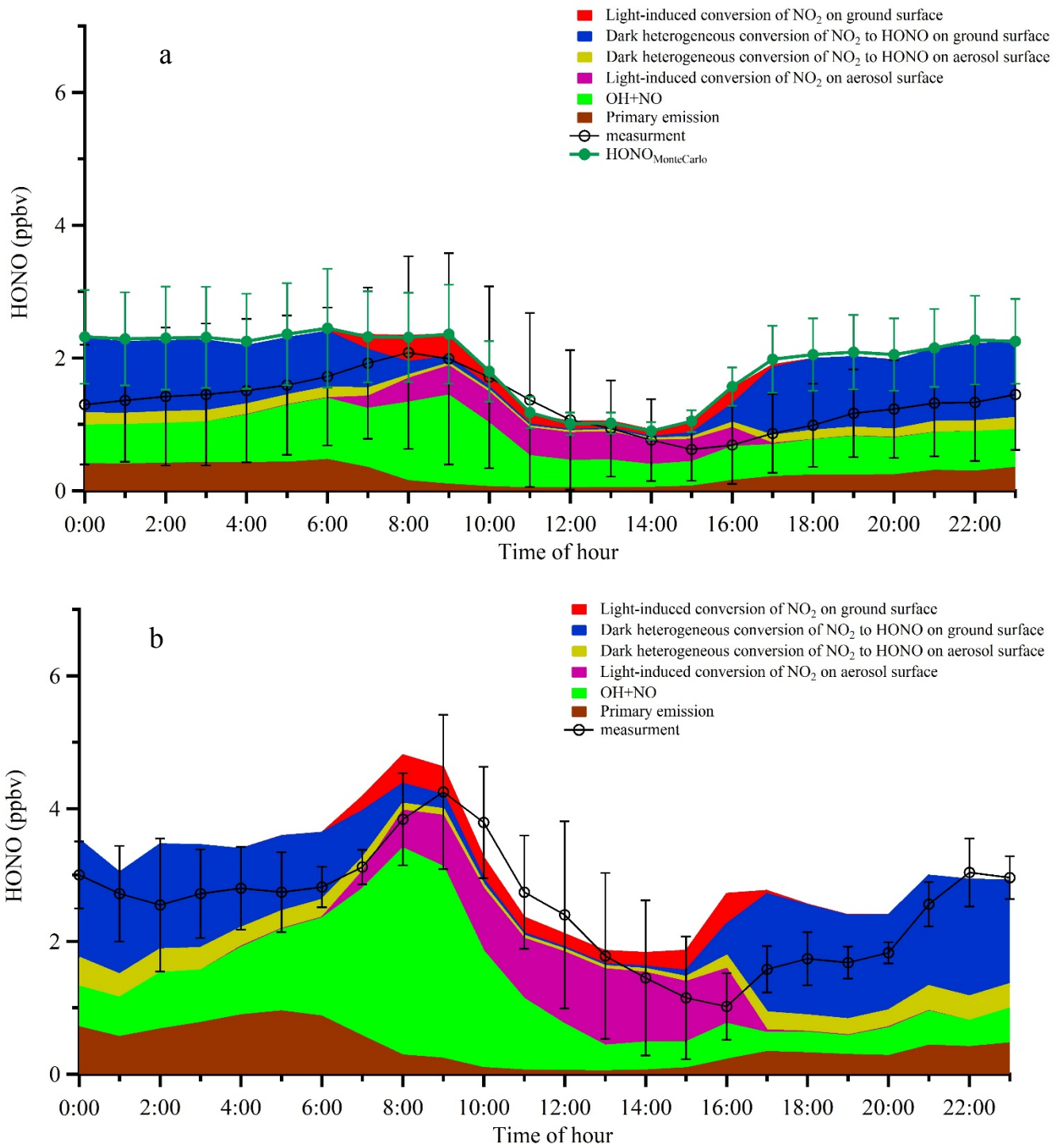
930



931

932 **Figure 9.** Averaged production and loss rates of daytime HONO and $J(\text{NO}_2)$ during the measurement period. The

933 black line shows the photolysis rate of NO_2 .



934 **Figure 10.** a) Averaged diurnal profiles of the measured HONO and the modeled HONO from different sources.
 935 Error bars on the black line represent standard deviations of HONO measurements in hourly bins. Error bars on the
 936 green markers denote the Monte Carlo analysis results; b) The same plot as panel a, except that only the two
 937 industrial plume events (the 7th and from the 21st to 22nd of December 2015) were considered in the model.
 938